Computing Spectral Measures of Self-Adjoint Operators*

Matthew Colbrook[†]
Andrew Horning[‡]
Alex Townsend[§]

Abstract. Using the resolvent operator, we develop an algorithm for computing smoothed approximations of spectral measures associated with self-adjoint operators. The algorithm can achieve arbitrarily high orders of convergence in terms of a smoothing parameter for computing spectral measures of general differential, integral, and lattice operators. Explicit pointwise and L^p -error bounds are derived in terms of the local regularity of the measure. We provide numerical examples, including a partial differential operator and a magnetic tight-binding model of graphene, and compute 1000 eigenvalues of a Dirac operator to near machine precision without spectral pollution. The algorithm is publicly available in SpecSolve, which is a software package written in MATLAB.

Key words. spectrum, spectral measures, resolvent, spectral methods, rational kernels

AMS subject classifications. 47A10, 46N40, 47N50, 65N35, 81Q10

DOI. 10.1137/20M1330944

Contents

I	Introduction	490
2	The Spectral Measure of a Self-Adjoint Operator	49 I
3	Applications of Spectral Measures 3.1 Particle and Condensed Matter Physics	492
	3.2 Time Evolution and Spectral Density Estimation	
1	4.1 Evaluating the Spectral Measure of an Integral Operator	
	4.2 Pointwise Convergence of Smoothed Measure	

^{*}Received by the editors April 13, 2020; accepted for publication (in revised form) December 18, 2020; published electronically August 5, 2021.

https://doi.org/10.1137/20M1330944

Funding: The work of the first author was supported by EPSRC grant EP/L016516/1. The work of the second and third authors was supported by the National Science Foundation through grant 1818757.

[†]Department of Applied Mathematics and Theoretical Physics, University of Cambridge, Cambridge, CB3 0WA, UK (m.colbrook@damtp.cam.ac.uk).

[‡]Center for Applied Mathematics, Cornell University, Ithaca, NY 14853 USA (ajh326@cornell.edu).

[§]Department of Mathematics, Cornell University, Ithaca, NY 14850 USA (townsend@cornell.edu).

5	High-Order Kernels					
	5.1	Rational Kernels	502			
		5.1.1 Equispaced Poles	504			
	5.2	Other Types of Convergence				
6	The	Resolvent Framework in Practice	508			
	6.1	Ordinary Differential Operators	508			
	6.2	Integral Operators	509			
	6.3	Infinite Sparse Matrices				
7	Exa	mples	511			
	7.1	Example 1: Beam and Two-Dimensional Schrödinger Equations	511			
	7.2	Example 2: The Schrödinger Equation on a Graphene Lattice				
		7.2.1 The Model	511			
		7.2.2 The Computed Measures				
	7.3	Example 3: Discrete Spectra and Dirac Operators	513			
		7.3.1 Recovering Eigenvalues and Projections onto Eigenspaces	514			
		7.3.2 The Dirac Operator	514			
		7.3.3 Computing Eigenvalues while Avoiding Spectral Pollution	515			
8	Cor	clusions and Additional Potential Applications	516			
Αį	pen	dix A. Convergence Rates and Error Bounds	516			
	A.1	Pointwise Error Bounds	516			
	A.2	L^p Error Bounds	518			
Αd	knov	vledgments	520			
Re	References					

1. Introduction. The spectrum of a finite matrix consists only of discrete eigenvalues; however, many of the infinite-dimensional operators in mathematical analysis and physical applications include a continuous spectral component [60, 100]. Notably, eigenvalues and eigenvectors do not diagonalize operators with continuous spectra, and one needs extra information to fully describe the operator and associated dynamics of physical models [47, 109]. Given a self-adjoint operator \mathcal{L} acting on a Hilbert space \mathcal{H} , the spectral measure (see (2.2)) of \mathcal{L} is a quantity of great interest because it provides an analogue of diagonalization through the spectral theorem (see section 2). Spectral measures are related to correlation in stochastic processes and signal-processing [44, 59], [89, Chap. 7], scattering cross-sections in particle physics [33, 34, 35], the local density-of-states in crystalline materials [5, 50, 70], and many other quantities [25, 28, 62, 114, 119]. Furthermore, through spectral measures one can compute the functional calculus of \mathcal{L} , which is used to solve evolution equations such as the Schrödinger equation in quantum mechanics [52, 72].

The eigenvalues and eigenvectors of an infinite-dimensional operator with discrete spectrum are usually computed by discretizing and employing a matrix eigensolver [9, 13]. Computing spectral measures is more subtle, and previous efforts have mainly focused on operators for which analytical formulas or heuristics are available (see section 3). Building on [16, 55], we develop a general framework for computing

approximations to spectral measures of operators that requires only two capabilities:

- 1. A numerical solver for shifted linear equations, i.e., $(\mathcal{L}-z)u=f$ with $z\in\mathbb{C}$.
- 2. Numerical approximations to inner products of the form $\langle u, f \rangle$.

Here, $\langle \cdot, \cdot \rangle$ is the inner product associated with \mathcal{H} , which can be general, provided one can compute $\langle u, f \rangle$. We develop high-order rational convolution kernels that allow us to construct accurate approximations to spectral measures by solving the shifted linear equations (see Table 5.1 and Figure 5.1). Error bounds show that our approximations to the spectral measure converge rapidly (see Theorems 5.2 and 5.3). We apply our algorithm to differential (see subsection 7.1), integral (see subsection 4.1), and lattice (see subsection 7.2) operators to demonstrate its versatility, high accuracy, and robustness. We also use our approximations of spectral measures to compute the first thousand eigenvalues of a Dirac operator (corresponding to bound states in the gap of the essential spectrum) without spectral pollution (see subsection 7.3). Thus, spectral measures are also a useful tool for the computation of discrete spectra when there are gaps in the essential spectrum or when discrete spectra cluster (see subsections 7.2 and 7.3). To accompany this paper, we have developed a publicly available MATLAB package called SpecSolve for computing spectral measures of a large class of self-adjoint operators [20].

The paper is organized as follows. We recall the definition of the spectral measure of an operator in section 2 and survey existing algorithms in section 3. In section 4, we introduce our computational framework, and we derive high-order versions in section 5. In section 6 we discuss algorithmic issues, and in section 7 tackle challenging applications. Finally, we point out additional capabilities and uses of the algorithm in section 8.

2. The Spectral Measure of a Self-Adjoint Operator. Any linear operator acting on a finite-dimensional Hilbert space has a purely discrete spectrum consisting of eigenvalues. In particular, the spectral theorem for self-adjoint $A \in \mathbb{C}^{n \times n}$ states that there exists an orthonormal basis of eigenvectors v_1, \ldots, v_n for \mathbb{C}^n such that

$$(2.1) \quad v = \left(\sum_{k=1}^n v_k v_k^*\right) v, \quad v \in \mathbb{C}^n, \quad \text{and} \quad Av = \left(\sum_{k=1}^n \lambda_k v_k v_k^*\right) v, \quad v \in \mathbb{C}^n,$$

where $\lambda_1, \ldots, \lambda_n$ are eigenvalues of A, i.e., $Av_k = \lambda_k v_k$ for $1 \le k \le n$. In other words, the projections $v_k v_k^*$ decompose \mathbb{C}^n and diagonalize A.

In the infinite-dimensional setting, we replace $v \in \mathbb{C}^n$ by $f \in \mathcal{H}$, and A by a self-adjoint operator \mathcal{L} with domain $\mathcal{D}(\mathcal{L}) \subset \mathcal{H}$. If \mathcal{L} has nonempty continuous spectrum, then eigenfunctions of \mathcal{L} do not form a basis for \mathcal{H} or diagonalize \mathcal{L} . However, the spectral theorem for self-adjoint operators states that the projections $v_k v_k^*$ in (2.1) can be replaced by a projection-valued measure \mathcal{E} [87, Thm. VIII.6]. The measure \mathcal{E} assigns an orthogonal projector to each Borel-measurable set such that

$$f = \left(\int_{\mathbb{R}} d\mathcal{E}(y)\right) f, \quad f \in \mathcal{H}, \quad \text{and} \quad \mathcal{L}f = \left(\int_{\mathbb{R}} y \, d\mathcal{E}(y)\right) f, \quad f \in \mathcal{D}(\mathcal{L}).$$

Analogous to (2.1), \mathcal{E} decomposes \mathcal{H} and diagonalizes the operator \mathcal{L} .

The spectral measure of \mathcal{L} with respect to $f \in \mathcal{H}$ is a scalar measure defined as $\mu_f(\Omega) := \langle \mathcal{E}(\Omega)f, f \rangle$, where $\Omega \subset \mathbb{R}$ is a Borel-measurable set [87]. It is useful to

¹Considering $\mathcal{L}: \mathcal{D}(\mathcal{L}) \to \mathcal{H}$ allows us to treat unbounded operators such as differential operators.

examine Lebesgue's decomposition of μ_f [97], i.e.,

(2.2)
$$d\mu_f(y) = \underbrace{\sum_{\lambda \in \Lambda^{\mathcal{P}}(\mathcal{L})} \langle \mathcal{P}_{\lambda} f, f \rangle \, \delta(y - \lambda) dy}_{\text{discrete part}} + \underbrace{\rho_f(y) \, dy + d\mu_f^{(\text{sc})}(y)}_{\text{continuous part}}.$$

The discrete part of μ_f is a sum of Dirac delta distributions, supported on the set of eigenvalues of \mathcal{L} , which we denote by $\Lambda^{\mathrm{p}}(\mathcal{L})$. The coefficient of each δ in the sum is $\langle \mathcal{P}_{\lambda} f, f \rangle = \|\mathcal{P}_{\lambda} f\|^2$, where \mathcal{P}_{λ} is the orthogonal spectral projector associated with the eigenvalue λ , and $\|\cdot\| = \sqrt{\langle \cdot, \cdot \rangle}$ is the norm on \mathcal{H} . The continuous part of μ_f consists of an absolutely continuous² part with Radon–Nikodym derivative $\rho_f \in L^1(\mathbb{R})$ and a singular continuous component $\mu_f^{(\mathrm{sc})}$. Without loss of generality, we assume throughout that $\|f\| = 1$, which ensures that μ_f is a probability measure.

Many operators have nonempty continuous spectra [60, Chap. 10] such as self-adjoint Toeplitz operators on $\ell^2(\mathbb{N})$ (square summable sequences, where $\mathbb{N} = \{1, 2, \ldots\}$) [8], differential operators on bounded domains with singular variable coefficients [45, 67] and unbounded domains [108, Chap. V], [31, Chap. XIII, Chap. XIV], and integral perturbations of multiplication operators and Cauchy-type integral operators [38, 63]. In physical systems that scatter or radiate energy, the associated operator typically has a mix of continuous and discrete spectra; e.g., see the RAGE theorem [2, 36, 90]. We aim to evaluate smoothed approximations of μ_f when $\mathcal L$ has a nonempty continuous spectrum. This means that we compute samples from a smooth function g_{ϵ} , with smoothing parameter $\epsilon > 0$, that converges weakly to μ_f [6, Chap. 1]. That is,

$$\int_{\mathbb{R}} \phi(y) g_{\epsilon}(y) dy \to \int_{\mathbb{R}} \phi(y) d\mu_f(y) \quad \text{as} \quad \epsilon \downarrow 0$$

for any bounded, continuous function ϕ . Approximation properties and explicit convergence bounds are studied in sections 4 and 5.

- **3. Applications of Spectral Measures.** Spectral measures appear in many traditional topics of applied analysis, such as ordinary differential equations (ODEs) and partial differential equations (PDEs), stochastic processes, orthogonal polynomials, and random matrix theory. Here, we give a brief survey of existing algorithms for computing μ_f and closely related quantities.
- 3.1. Particle and Condensed Matter Physics. Spectral measures are prominent in quantum mechanics [48, 87], where a self-adjoint operator \mathcal{L} represents an observable quantity, and μ_f describes the likelihood of different outcomes when the observable is measured (see subsection 5.2). In this setting, $f \in \mathcal{H}$ with ||f|| = 1 represents a quantum state. For example, in quantum models of interacting particles, spectral measures of many-body Hamiltonians are used to study the response of a quantum system to perturbations [33]. In condensed matter physics, spatially resolved statistical properties of materials are analyzed using the local density-of-states³ (LDOS) of an $n \times n$ matrix A_n [61, sect. 6.4], which is the spectral measure of A_n taken with respect to a vector b [70]. Here, A_n is typically a discretized or truncated Hamiltonian, and one is interested in the thermodynamic limit $n \to \infty$, so that A_n is too large to compute a full eigenvalue decomposition.

²We take "absolutely continuous" to be with respect to Lebesgue measure.

³This is distinct from the global density-of-states (DOS), which is formally obtained from the LDOS via an averaging procedure [61, sect. 6.4].

There are two main classes of numerical methods for computing these measures. One class constructs smooth global approximations of the measure with explicit moment-matching procedures [66, 92, 118], while another class exploits a connection between the spectral measure and the resolvent operator to evaluate samples from a smoothed approximation to the measure [5, 34, 50]. For example, the so-called recursion method [5, 50] evaluates the resolvent of tridiagonal Hamiltonians using associated continued-fraction expansions. Resolvent techniques to compute the DOS of finite matrices also appear in the study of random matrices and Schrödinger operators, where the connection is made through the Stieltjes transform [4, 10].

The resolvent of an operator \mathcal{L} with spectrum $\Lambda(\mathcal{L})$ is given by [60, p. 173]

(3.1)
$$\mathcal{R}_{\mathcal{L}}(z) = (\mathcal{L} - z)^{-1}, \qquad z \in \mathbb{C} \setminus \Lambda(\mathcal{L}).$$

In section 4, we evaluate a smoothed approximation of μ_f by evaluating the resolvent function $\langle \mathcal{R}_{\mathcal{L}}(z)f, f \rangle$ in the upper half-plane, i.e., $\operatorname{Im}(z) > 0$. Our approach is closely related to the second class of methods developed for operators in quantum mechanics. A key theme in the above moment-matching and resolvent-based approaches is smoothing, which is introduced by convolution with a smoothing kernel to avoid difficulties associated with the singular part of the measure [70]. The smoothed approximations of the spectral measures that we compute in sections 4 and 5 also have the form of $K_{\epsilon} * \mu_f$, where K_{ϵ} is a smoothing kernel with smoothing parameter $\epsilon > 0$.

Our framework is "discretization-oblivious" in the sense that it directly resolves the spectral measure of an infinite-dimensional \mathcal{L} , and not an underlying discretization. This means that our algorithms do not suffer from spectral pollution.⁴ Moreover, our framework can be used with any accurate numerical method for solving linear operator equations and computing inner products, making it applicable to differential, integral, and lattice operators. Achieving a discretization-oblivious framework requires balancing refinement in the computation of $\langle \mathcal{R}_{\mathcal{L}}(z)f, f \rangle$ and refinement in the smoothing parameter, which we do in a principled way (see subsection 4.3).

3.2. Time Evolution and Spectral Density Estimation. Spectral measures provide a useful lens when studying processes that evolve over time. Suppose that $u:[0,T] \to \mathcal{H}$ evolves over time according to the abstract Cauchy problem

(3.2)
$$\frac{du}{dt} = -i\mathcal{L}u, \qquad u(0) = f \in \mathcal{H},$$

where \mathcal{L} is a self-adjoint operator. For example, (3.2) could describe the evolution of a quantum system according to the Schrödinger equation [72]. Semigroup theory [81] shows that the solution to (3.2) is given by the operator exponential $e^{-i\mathcal{L}t}f$. The autocorrelation function of u is of interest, i.e.,

$$\langle u(t), f \rangle = \langle e^{-i\mathcal{L}t} f, f \rangle = \int_{\mathbb{R}} e^{-iyt} d\mu_f(y), \qquad t \in [0, T],$$

which can reveal features that persist over time [105]. This interpretation of a time evolution process is quite flexible and can be adapted to describe many signals, u, generated by PDEs [27, 56, 94] and stochastic processes [44, 59], [89, Chap. 7].

In certain evolution processes, μ_f is referred to as the spectral density of u [22]. The task of spectral density estimation is to recover μ_f from samples of u(t) [99,

⁴Spectral pollution is the phenomenon of eigenvalues of finite discretizations/truncations clustering at points not in the spectrum of \mathcal{L} as the truncation size increases.

sect. 1.5]. A popular technique used in spectral density estimation, related to statistical kernel density estimation [115, 116], reconstructs a smoothed approximation to μ_f by convolving the empirical measure (a discrete measure supported on the observed samples) with a smoothing kernel [78, 83]. The particular choice of smoothing kernel affects the convergence properties of the smoothed spectral density [79].

In analogy to the variance-bias tradeoff encountered when selecting the smoothing parameter in statistical kernel density estimation [80, 88], our smoothed approximations, $K_{\epsilon} * \mu_f$, exhibit a tradeoff between numerical cost and smoothing (see subsection 4.3). In section 5, we adapt arguments from kernel density estimation to determine what properties a smoothing kernel needs to achieve a high order of convergence in the smoothing parameter.

3.3. Sturm–Liouville and Jacobi Operators. Spectral density functions are used in the analysis of singular Sturm–Liouville problems and related classes of self-adjoint operators [73]. A subtle distinction between spectral measures μ_f and the spectral density function associated with a Sturm–Liouville problem is that the latter does not depend on a given vector f. Instead, the spectral density function corresponds to the multiplicative version of the spectral theorem [87, Thm. VIII.4], which induces a Fourier transform–type pair [15]. However, computational methods for both spectral quantities share similarities. For example, one can compute spectral density functions using a Plemelj-type formula [119], which is similar to (4.1).

A common approach to computing spectral density functions associated with Sturm-Liouville operators on unbounded domains is to truncate the domain and take an appropriate limit of an eigenvalue counting function, as implemented in the software package SLEDGE [41, 42, 84]. This is similar in spirit to DOS calculations, though convergence analysis remains challenging due to the truncation of the infinite interval [85]. This approach can be computationally expensive since the eigenvalues cluster as the domain size increases; often, hundreds of thousands of eigenvalues and eigenvectors need to be computed. One can avoid this cost for certain operators by leveraging analytic limit formulas and solving an ODE at each evaluation point of the spectral density function [39, 40]. Similar methods apply to compute the inverse scattering transform for the Toda lattice and the KdV equation [7, 114].

For a Jacobi operator J on $\ell^2(\mathbb{N})$, under suitable conditions [106, Chap. 2], the spectral measure μ_{e_1} of J (e_1 denotes the first canonical basis vector) coincides with the measure given by the multiplicative version of the spectral theorem. Moreover, μ_{e_1} is the probability measure associated with the orthonormal polynomials whose three-term recurrence relation is associated with J [26]. Due to this connection, the study of spectral measures has a rich history in the theory of orthogonal polynomials and quadrature rules for numerical integration [26, 28, 69, 103, 106]. In special cases, one can recover a distribution function for μ_{e_1} as a limit of functions constructed using Gaussian quadrature [14, Chap. 2]. One can even use connection coefficients between families of orthogonal polynomials to compute spectral measures of Jacobi operators that arise as compact perturbations of Toeplitz operators [117]. Applications in this direction include quantum theory and random matrix theory [43, 62, 95].

While these approaches are specialized to a selected class of operators, we focus on developing a general framework to deal rigorously with arbitrary order ODEs and PDEs (see subsection 7.1) and integral operators (see subsection 4.1). The price we pay for this generality is the need to solve shifted linear systems close to the operator's spectrum. We demonstrate that this can be done robustly with fast, well-conditioned, and spectrally accurate methods (see section 6). Similarly, we aim

to build a framework that treats general discrete or lattice operators (see subsection 6.3).

4. Resolvent-Based Approach to Evaluate the Spectral Measure. The key to our framework for computing spectral measures is the resolvent of \mathcal{L} (see (3.1)). A classical result in operator theory is Stone's formula, which says that the spectral measure of \mathcal{L} can be recovered from the jump in the resolvent $\mathcal{R}_{\mathcal{L}}(z)$ across the real axis [101], [87, Thm. VII.13]. More precisely, if we select $\epsilon > 0$ and regard $\mathcal{R}_{\mathcal{L}}(x + i\epsilon)$ as a function of the real variable x, then we have that

$$(4.1) \quad \frac{1}{2\pi i} \langle (\mathcal{R}_{\mathcal{L}}(\cdot + i\epsilon) - \mathcal{R}_{\mathcal{L}}(\cdot - i\epsilon))f, f \rangle = \frac{1}{\pi} \operatorname{Im}(\langle \mathcal{R}_{\mathcal{L}}(\cdot + i\epsilon)f, f \rangle) \to \mu_f \text{ as } \epsilon \downarrow 0.$$

Here, the equality is due to the conjugate symmetry of $\mathcal{R}_{\mathcal{L}}(z)$ across the real axis and the limit should be understood in the sense of weak convergence of measures.

Stone's formula is a consequence of the functional calculus identity

(4.2)
$$\langle \mathcal{R}_{\mathcal{L}}(x+i\epsilon)f, f \rangle = \int_{\mathbb{R}} \frac{d\mu_f(y)}{y - (x+i\epsilon)}.$$

By using (4.2) to rewrite (4.1), we arrive at an expression for the jump over the real axis as a convolution of the spectral measure with the Poisson kernel, i.e.,

(4.3)
$$\frac{1}{\pi} \operatorname{Im}(\langle \mathcal{R}_{\mathcal{L}}(x+i\epsilon)f, f \rangle) = \frac{1}{\pi} \int_{\mathbb{R}} \frac{\epsilon}{\epsilon^2 + (x-y)^2} d\mu_f(y).$$

The Poisson kernel is one of the most common kernels used to smooth approximations of measures in particle and condensed matter physics (see the discussion in subsection 3.1). When \mathcal{L} has no singular continuous spectrum, substituting the spectral measure given in (2.2) into the expression (4.3) shows that $\mathcal{R}_{\mathcal{L}}(x+i\epsilon)$ provides an approximation to both the discrete and the continuous components of the measure μ_f for $\epsilon > 0$. That is,

$$(4.4) \quad \frac{1}{\pi} \operatorname{Im}(\langle \mathcal{R}_{\mathcal{L}}(x+i\epsilon)f, f \rangle) = \frac{1}{\pi} \sum_{\lambda \in \Lambda^{p}(\mathcal{L})} \frac{\epsilon \langle \mathcal{P}_{\lambda}f, f \rangle}{\epsilon^{2} + (x-\lambda)^{2}} + \frac{1}{\pi} \int_{\mathbb{R}} \frac{\epsilon \rho_{f}(y)}{\epsilon^{2} + (x-y)^{2}} \, dy.$$

The contribution from the sum in (4.4) is a series of Poisson kernels centered at the eigenvalues and scaled by the corresponding coefficients $\langle \mathcal{P}_{\lambda} f, f \rangle$ for $\lambda \in \Lambda^{p}(\mathcal{L})$. As $\epsilon \downarrow 0$, the sum converges to a series of Dirac delta distributions representing the discrete part of the measure in (2.2). Meanwhile, the integral in (4.4) contributes a smoothed approximation to the Radon–Nikodym derivative ρ_f .

Motivated by (4.4), we select $\epsilon > 0$ and approximate samples of μ_f by evaluating

(4.5)
$$\mu_f^{\epsilon}(x) := \frac{1}{\pi} \operatorname{Im}(\langle \mathcal{R}_{\mathcal{L}}(x + i\epsilon) f, f \rangle).$$

From (4.1), we know that as $\epsilon \downarrow 0$ we have $\mu_f^{\epsilon} \to \mu_f$ in the sense of weak convergence of measures. Moreover, if μ_f has some additional local regularity about a point $x_0 \in \mathbb{R}$, then $\mu_f^{\epsilon}(x_0) \to \rho_f(x_0)$ as $\epsilon \downarrow 0$ (see Theorem 4.1). There is a two-step procedure for evaluating $\mu_f^{\epsilon}(x_0)$ at some $x_0 \in \mathbb{R}$, which is immediate from (4.5):

1. Solve the shifted linear equation for u^{ϵ} :

$$(4.6) (\mathcal{L} - x_0 - i\epsilon)u^{\epsilon} = f, u^{\epsilon} \in \mathcal{D}(\mathcal{L}).$$

2. Compute the inner product $\mu_f^{\epsilon}(x_0) = \frac{1}{\pi} \text{Im}(\langle u^{\epsilon}, f \rangle)$.

In practice, the smaller $\epsilon > 0$, the more computationally expensive it is to evaluate (4.5) because if $x_0 \in \Lambda(\mathcal{L})$, then the resolvent operator $\mathcal{R}_{\mathcal{L}}(x_0 + i\epsilon)$ is unbounded in the limit $\epsilon \downarrow 0$. One often computes $\mu_f^{\epsilon}(x_0)$ for successively smaller ϵ to obtain a sequence that converges to $\mu_f(x_0)$. For example, Richardson's extrapolation can improve the convergence rate in ϵ [16], which can be proven using the machinery of section 5.

Typically, one wants to sample μ_f^ϵ at several points $x_1,\ldots,x_m\in\mathbb{R}$ and then construct a local or global representation of μ_f^ϵ for visualization or further computations. If one wants to visualize μ_f^ϵ in an interval, then we recommend evaluating at equispaced points in that interval. However, when one wants to calculate an integral with respect to μ_f^ϵ , it is better to evaluate μ_f^ϵ at quadrature nodes (see subsection 5.2). Note that if $x_j \notin \Lambda(\mathcal{L})$, then $\mu_f^\epsilon(x_j) \to 0$ as $\epsilon \downarrow 0$ (for example, see Figure 4.1).

Although the singular continuous spectrum may appear to be an exotic phenomenon, it occurs in applications of practical interest. For example, discrete Schrödinger operators with aperiodic potentials on $\ell^2(\mathbb{Z})$ (such as the Fibonacci Hamiltonian) can have spectra that are Cantor sets with purely singular continuous spectral measures (see [3, 23, 24, 46, 86, 102]). When $\Lambda(\mathcal{L})$ has a nonzero singular continuous component, $\mu_f^{\epsilon} \to \mu_f$ weakly as $\epsilon \downarrow 0$ and our algorithms can compute $\mu_f(U)$ (for open sets U) and the functional calculus of \mathcal{L} .

4.1. Evaluating the Spectral Measure of an Integral Operator. To illustrate our evaluation strategy, consider the integral operator defined by

$$(4.7) \quad [\mathcal{L}u](x) = xu(x) + \int_{-1}^{1} e^{-(x^2 + y^2)} u(y) \, dy, \qquad x \in [-1, 1], \qquad u \in L^2([-1, 1]).$$

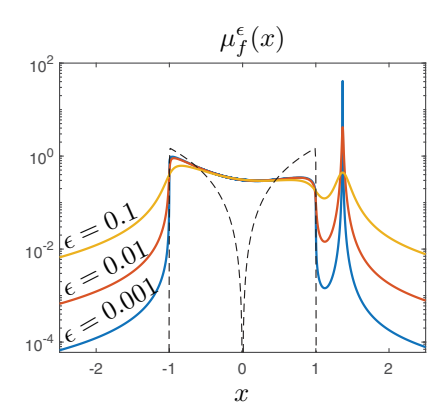
The integral operator \mathcal{L} in (4.7) has continuous spectrum in [-1,1], due to the xu(x) term, and discrete spectrum in $\mathbb{R} \setminus [-1,1]$ from the integral term (a compact perturbation [60]). Figure 4.1 (left) shows three smoothed approximations of μ_f with $f(x) = \sqrt{3/2} x$, for smoothing parameter $\epsilon = 0.1, 0.01$, and 0.001. We see the presence of an eigenvalue near $x \approx 1.37$ from a spike in the smoothed measure that approximates a Dirac delta.

To perform the two-step procedure described above on a computer, we must discretize the operator \mathcal{L} , and we do this by discretizing \mathcal{L} with an $N \times N$ matrix corresponding to an adaptive Chebyshev collocation scheme.⁶ While the precise discretization details are delayed until subsection 6.2, Figure 4.1 illustrates the critical role that N plays when evaluating μ_f^{ϵ} . In particular, there are two limits to take in theory: $N \to \infty$ and $\epsilon \downarrow 0$. It is known that these two limits must be taken with considerable care [16]. If N is kept fixed as one takes $\epsilon \downarrow 0$, then the computed samples of μ_f^{ϵ} do not converge (see Figure 4.1 (right)) because they get polluted by the discrete spectrum of the discretization. Instead, as one takes $\epsilon \downarrow 0$, one must appropriately increase N too. In practice, we increase N by selecting it adaptively to ensure that we adequately resolve solutions to (4.6) (see Figure 4.1 (left)). The precise details on how we adequately resolve solutions are given in subsection 6.2.

4.2. Pointwise Convergence of Smoothed Measure. It is known that if μ_f is locally absolutely continuous with continuous Radon–Nikodym derivative ρ_f (see (2.2)),

⁵In general, it is also impossible to design a black-box method that separates the singular continuous component of μ_f from the other components. This is made precise in [16], which uses the framework of the solvability complexity index (SCI) hierarchy [17, 18, 19].

⁶While $N \times N$ discretizations converge for Fredholm operators [57], square truncations of spectral discretizations of operators may not always converge. Instead, one may need to take rectangular truncations to ensure that discretizations of $\mathcal{R}_{\mathcal{L}}(z)f$ converge [16].



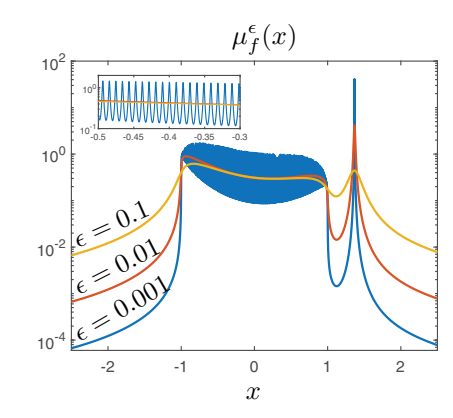


Fig. 4.1 Left: The smoothed approximation μ_f^ϵ for the integral operator in (4.7) and different ϵ . The discretization sizes for solving the shifted linear systems are adaptively selected. The dashed line corresponds to the spectral measure of the operator given by $u(x) \to xu(x)$. Adding the compact perturbation (the integral term) alters the shape of the measure over [-1,1], and there is an additional eigenvalue near $x\approx 1.37$. Right: The same computation except with a fixed discretization size of N=300 to solve (4.6). The magnified region shows spurious high-frequency oscillations for $\epsilon=0.001$, an artifact caused by the discrete spectrum of the underlying discretization.

then μ_f^{ϵ} converges pointwise to ρ_f [53, p. 22]. However, under additional smoothness assumptions on μ_f , it is useful to understand how rapidly μ_f^{ϵ} converges to μ_f . The connection between μ_f^{ϵ} and the Poisson kernel in (4.3) allows us to do this on intervals for which μ_f possesses some local regularity so that ρ_f is Hölder continuous. We let $\mathcal{C}^{k,\alpha}(I)$ denote the Hölder space of functions that are k times continuously differentiable on an interval I with an α -Hölder continuous kth derivative [37]. For $h_1 \in \mathcal{C}^{0,\alpha}(I)$ and $h_2 \in \mathcal{C}^{k,\alpha}(I)$ we define the seminorm and norm, respectively, as

$$|h_1|_{\mathcal{C}^{0,\alpha}(I)} = \sup_{x \neq y \in I} \frac{|h_1(x) - h_1(y)|}{|x - y|^{\alpha}}, \quad ||h_2||_{\mathcal{C}^{k,\alpha}(I)} = |h_2^{(k)}|_{\mathcal{C}^{0,\alpha}(I)} + \max_{0 \leq j \leq k} ||h_2^{(j)}||_{\infty,I}.$$

THEOREM 4.1. Suppose that the measure μ_f in (2.2) is absolutely continuous on the interval $I = (x_0 - \eta, x_0 + \eta)$ for some $x_0 \in \mathbb{R}$ and $\eta > 0$, let μ_f^{ϵ} be defined as in (4.5), and let $0 \le \alpha < 1$. If $\rho_f \in \mathcal{C}^{0,\alpha}(I)$, then

$$|\rho_f(x_0) - \mu_f^{\epsilon}(x_0)| = \mathcal{O}(\epsilon^{\alpha})$$
 as $\epsilon \downarrow 0$.

Proof. First, decompose ρ_f into two nonnegative parts so that $\rho_f = \rho_1 + \rho_2$, where the support of ρ_1 is in I and ρ_2 vanishes on $(x_0 - \eta/2, x_0 + \eta/2)$. Since $\rho_f(x_0) = \rho_1(x_0)$ and the Poisson kernel integrates to 1, we can use the convolution representation for μ_f^{ϵ} (see (4.3) and (4.5)) and the commutativity of convolution to bound the approximation error as

Here, $d\mu_f^{(r)}(y) := d\mu_f(y) - \rho_1(y)dy$ is a nonnegative measure with support in $\mathbb{R} \setminus (x_0 - \eta/2, x_0 + \eta/2)$. Since μ_f is a probability measure, we have that $\int_{\mathbb{R}} d\mu_f^{(r)}(y) \leq 1$, and

the second term in (4.8) is bounded via

(4.9)
$$\int_{\mathbb{R}} \frac{\epsilon d\mu_f^{(r)}(y)}{\epsilon^2 + (x_0 - y)^2} = \int_{|x_0 - y| \ge \eta/2} \frac{\epsilon d\mu_f^{(r)}(y)}{\epsilon^2 + (x_0 - y)^2} \le \frac{\epsilon}{\epsilon^2 + \frac{\eta^2}{4}}.$$

Since $\rho_f \in \mathcal{C}^{0,\alpha}(I)$, standard arguments using cutoff functions [37] show that we can choose ρ_1 so that $|\rho_1|_{\mathcal{C}^{0,\alpha}(I)} \leq |\rho_f|_{\mathcal{C}^{0,\alpha}(I)} + C\eta^{-\alpha} ||\rho_f||_{\infty,I}$ for some universal constant C. Consequently, we have that

$$|\rho_1(x_0) - \rho_1(x_0 - y)| \le |\rho_1|_{\mathcal{C}^{0,\alpha}(I)} |y|^{\alpha} \le (|\rho_f|_{\mathcal{C}^{0,\alpha}(I)} + C\eta^{-\alpha} ||\rho_f||_{\infty,I}) |y|^{\alpha}.$$

Substituting this bound into the first term on the right-hand side of (4.8) and combining with (4.9) yields

$$|\rho_f(x_0) - \mu_f^{\epsilon}(x_0)| \le \frac{|\rho_f|_{\mathcal{C}^{0,\alpha}(I)} + C\eta^{-\alpha} \|\rho_f\|_{\infty,I}}{\pi} \int_{\mathbb{R}} \frac{\epsilon}{\epsilon^2 + y^2} |y|^{\alpha} dy + \frac{\epsilon}{\pi \left(\epsilon^2 + \frac{\eta^2}{4}\right)}.$$

Calculating the integral explicitly leads to

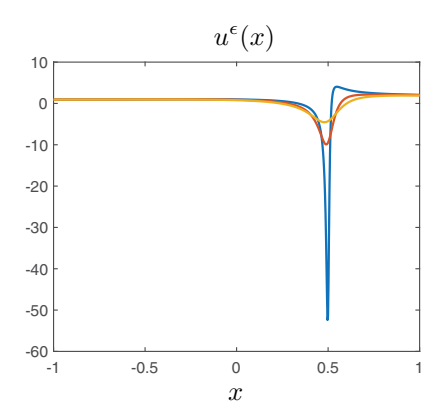
$$(4.10) |\rho_f(x_0) - \mu_f^{\epsilon}(x_0)| \le \left(|\rho_f|_{\mathcal{C}^{0,\alpha}(I)} + C\eta^{-\alpha} \|\rho_f\|_{\infty,I} \right) \sec\left(\frac{\alpha\pi}{2}\right) \epsilon^{\alpha} + \frac{\epsilon}{\pi \left(\epsilon^2 + \frac{\eta^2}{4}\right)}.$$

The right-hand side of (4.10) is $\mathcal{O}(\epsilon^{\alpha})$ as $\epsilon \downarrow 0$, which concludes the proof.

In Theorem 4.1, we see that the convergence rate of $|\rho_f(x_0) - \mu_f^{\epsilon}(x_0)|$ as $\epsilon \downarrow 0$ depends on the local regularity of μ_f . One can also show (see Theorem 5.2) that $|\rho_f(x_0) - \mu_f^{\epsilon}(x_0)| = \mathcal{O}(\epsilon \log(1/\epsilon))$ if $\rho_f \in \mathcal{C}^1(I)$ as well as the fact that any additional smoothness assumptions on ρ_f no longer improve the convergence rate.⁷ Since our procedure is local, the convergence rate is not affected by far away discrete and singular continuous components of μ_f . However, the convergence degrades near singular points in the spectral measure because the constants in (4.10) blow up as $\eta \to 0$. While $|\rho_f(x_0) - \mu_f^{\epsilon}(x_0)| = \mathcal{O}(\epsilon^{\alpha})$ in Theorem 4.1 is stated as an asymptotic statement, we can also obtain explicit bounds for adaptive selection of ϵ (see Theorem 5.2).

- **4.3. A Numerical Balancing Act.** To explore the practical importance of the convergence rates in Theorem 4.1, we examine the numerical cost associated with solving the shifted linear systems in (4.6). When the real component of the shift is in the continuous spectrum of \mathcal{L} and ϵ is small, we typically require large discretizations to avoid the situation observed in Figure 4.1 (right). There are many potential reasons why we require large discretization sizes as $\epsilon \downarrow 0$. Here are two illustrative examples:
- (I) Interior layers. Revisiting the integral operator example in (4.7), we select $x_0 = 1/2$ in the continuous spectrum of \mathcal{L} and $f(x) = \sqrt{3/2} x$. In Figure 4.2 (left), we observe that the solution $u^{\epsilon}(x)$ develops an interior layer and blows up at $x_0 = 1/2$ as $\epsilon \downarrow 0$. The blow-up occurs because the multiplicative term in $\mathcal{L} (x_0 + i\epsilon)$ has a root at $x_0 = 1/2$ when $\epsilon = 0$, giving rise to a pole in $u^{\epsilon}(x)$. For $\epsilon > 0$, the pole of $u^{\epsilon}(x)$ is located at a distance of $\mathcal{O}(\epsilon)$ away from the real axis. A large discretization size is needed to resolve $u^{\epsilon}(x)$ for small ϵ due to the thin interior layer in $u^{\epsilon}(x)$.

⁷The logarithmic term occurs due to the nonintegrability of $x/(\pi(x^2+1))$. One can also show that the error rate of $\mathcal{O}(\epsilon \log(1/\epsilon))$ is achieved if $\rho_f \in \mathcal{C}^{0,1}(I)$ is Lipschitz continuous.



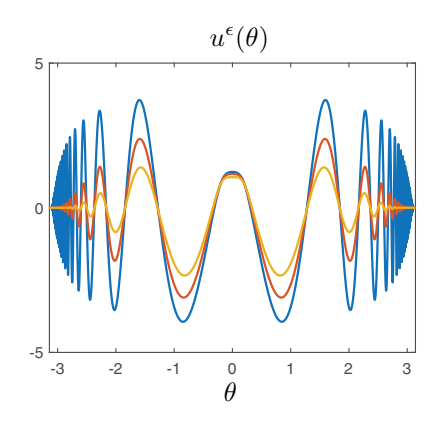


Fig. 4.2 Real part of the numerical solutions to the shifted linear equations in (4.6) for the integral operator in (4.7) (left) and the Schrödinger operator in (4.11) (right), with $\epsilon = 0.1$ (yellow), $\epsilon = 0.05$ (orange), and $\epsilon = 0.01$ (blue). The solutions to (4.11) are mapped to $[-\pi, \pi]$ via $x = 10i(1 - e^{i\theta})/(1 + e^{i\theta})$. We discretize using sparse, well-conditioned spectral methods, and the discretization sizes are selected adaptively to accurately resolve $u^{\epsilon}(x)$ and $u^{\epsilon}(\theta)$.

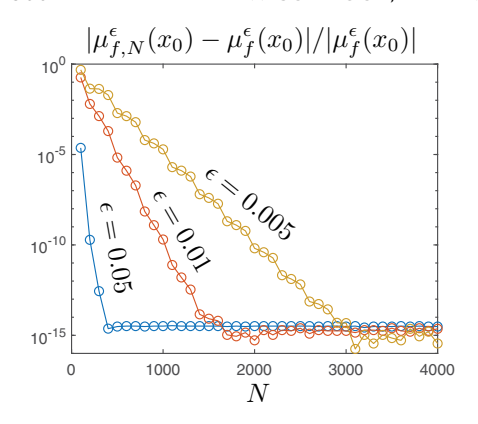
(2) Oscillatory behavior. Consider the second-order differential operator given by

(4.11)
$$[\mathcal{L}u](x) = -\frac{d^2u}{dx^2}(x) + \frac{x^2}{1+x^6}u(x), \qquad x \in \mathbb{R}.$$

We select $x_0 = 0.3$ in the continuous spectrum of \mathcal{L} , and $f(x) = \sqrt{9/\pi} \cdot x^2/(1+x^6)$. In Figure 4.2 (right), we plot solutions mapped onto the domain $[-\pi, \pi]$ by the change of variables $x = 10i(1-e^{i\theta})/(1+e^{i\theta})$. The solutions $u^{\epsilon}(x)$ are highly oscillatory with slow decay as $\theta \to \pm \pi$. As $\epsilon \downarrow 0$ the decay degrades and the persistent oscillations correspond to a transition in the nature of the singular points of (4.6) at $\pm \infty$. This means a large discretization is needed to resolve $u^{\epsilon}(x)$ for small ϵ .

The dominating computational expense in evaluating μ_f^{ϵ} is solving the shifted linear systems in (4.6), and the cost of computing $u^{\epsilon}(x)$ generally increases as $\epsilon \downarrow 0$. There is a balancing act. On the one hand, we wish to stay as far away from the spectrum as possible, so that the evaluation of μ_f^{ϵ} is computationally efficient. On the other hand, we desire samples of μ_f^{ϵ} to be good approximations to ρ_f , which requires a small $\epsilon > 0$. Even though we use sparse, well-conditioned spectral methods to discretize (4.6) (see section 6), the tradeoff between computational cost and accuracy means that the slow convergence rate determined in Theorem 4.1 is a severe limitation. In Figure 4.3, we explore the discretization sizes that are needed to evaluate spectral measures with the Poisson kernel accurately. For the integral operator in (4.7) and $\epsilon = 0.05$, 0.01, and 0.005, we observe that we need N = 400, 1700, and 3100, respectively (see Figure 4.3 (left)). Unfortunately, to obtain samples of the spectral measure with two digits of relative accuracy, we require that $\epsilon \approx 0.01$ (see Figure 4.3). For this example, we observe that we require $N \approx 20/\epsilon$ for small $\epsilon > 0$, so it is computationally infeasible to obtain more than five or six digits of accuracy with the Poisson kernel.

In addition to the computational cost of increasing N, the discretizations used to solve the linear systems in (4.6) become increasingly ill-conditioned when $x_0 \in \Lambda(\mathcal{L})$ and $\epsilon \downarrow 0$ (a reflection of $\|\mathcal{R}_{\mathcal{L}}(x_0+i\epsilon)\| = \epsilon^{-1}$). This can limit the attainable accuracy. Moreover, the performance of iterative methods, if used to accelerate the solution of the large shifted linear systems, may also suffer. In our experience, the cost of increasing N is usually the limiting factor and we rarely take $\epsilon < 10^{-2}$.



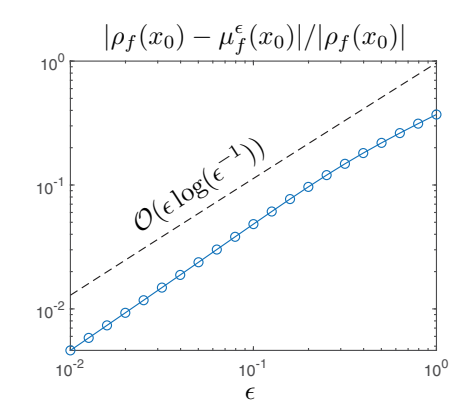


Fig. 4.3 Left: The relative error in the numerical approximation $\mu_{f,N}^{\epsilon}$, corresponding to discretization size N, of the smoothed measure in (4.5) for the integral operator in (4.7) with $\epsilon = 0.05$, $\epsilon = 0.01$, and $\epsilon = 0.005$. Right: The pointwise relative difference between the smoothed measure $\mu_f^{\epsilon}(x)$ and the density $\rho_f(x)$, evaluated at $x_0 = 1/2$, compared with the $\mathcal{O}(\epsilon \log(\epsilon^{-1}))$ error bound in Theorem 5.2 for the integral operator in (4.7). The relative error is computed by comparing with a numerical solution that has been adaptively resolved to machine precision.

5. High-Order Kernels. Theorem 4.1 demonstrates that $\mu_f^{\epsilon} \to \rho_f$ pointwise in intervals for which μ_f is absolutely continuous with Hölder continuous density ρ_f , where the rate of convergence depends on the Hölder exponent of ρ_f . However, even when ρ_f possesses additional regularity, the best rate of convergence for smoothed measures using the Poisson kernel is $\mathcal{O}(\epsilon \log(1/\epsilon))$. A natural question is:

"Can we use other kernels to exploit additional regularity in μ_f ?"

In this section, we construct kernels that can be used to compute smoothed measures that approximate ρ_f to high order in ϵ when ρ_f is smooth. This allows us to obtain accurate samples of μ_f while avoiding extremely small ϵ and the associated computational cost of solving the shifted linear equations in (4.6) when the shifts are close to the real line. We use K(x) to denote a kernel for which $K_{\epsilon}(x) = \epsilon^{-1}K(x/\epsilon)$ is an approximation to the identity, i.e., $K_{\epsilon} \to \delta$ as $\epsilon \downarrow 0$ in the sense of distributions [98, Chap. 3], where δ is the Dirac delta distribution.

To gain intuition about the conditions that K(x) must satisfy so that $K_{\epsilon} * \mu_f$ approximates μ_f to high order, consider an absolutely continuous probability measure μ with density ρ supported on an interval $I = (x_0 - \eta, x_0 + \eta)$ for some $x_0 \in \mathbb{R}$ and $\eta > 0$. The following argument is common in statistical nonparametric regression [115, 116]. Since we want K_{ϵ} to be an approximation to the identity, our first property is that $\int_{\mathbb{R}} K(x) dx = 1$. For further properties, we examine the approximation error

$$[K_{\epsilon} * \mu](x_0) - \rho(x_0) = \int_{\mathbb{R}} K_{\epsilon}(y) (\rho(x_0 - y) - \rho(x_0)) dy.$$

Assuming that $\rho \in \mathcal{C}^{n,\alpha}(I)$ for some $0 < \alpha < 1$, we can use an *n*th-order Taylor expansion of $\rho(x_0 - y) - \rho(x_0)$ to rewrite the approximation error as

$$[K_{\epsilon} * \mu](x_0) - \rho(x_0) = \sum_{k=1}^{n-1} \frac{(-1)^k \rho^{(k)}(x_0)}{k!} \int_{\mathbb{R}} K_{\epsilon}(y) y^k \, dy + \int_{\mathbb{R}} K_{\epsilon}(y) R_n(x_0, y) \, dy,$$

where $R_n(x_0, y)$ denotes the $\mathcal{O}(|y|^n)$ remainder term in the Taylor series and $\rho^{(k)}$ is the kth derivative of ρ . The change of variables $y \to \epsilon y$ reveals that the kth term in the series is of size $\mathcal{O}(\epsilon^k)$, provided that $K(y)y^k$ is integrable. Meanwhile, the Hölder continuity of $\rho^{(n)}$ shows that the term involving $R_n(x_0, y)$ is of size $\mathcal{O}(\epsilon^{n+\alpha})$, provided that $K(y)y^{n+\alpha}$ is integrable and $\int_{\mathbb{R}} K(y)y^n dy = 0$. Therefore, a kernel that achieves an $\mathcal{O}(\epsilon^{n+\alpha})$ approximation error has vanishing moments, i.e., $\int_{\mathbb{R}} K(y)y^k dy = 0$ for $1 \le k \le n$.

In practice, μ may not be absolutely continuous and its absolutely continuous part may have a density ρ with singular points or unbounded support. As in Theorem 4.1, we can deal with the general case by decomposing $\rho = \rho_1 + \rho_2$ into two nonnegative parts, where ρ_1 is sufficiently smooth and compactly supported on I, and where ρ_2 vanishes in a neighborhood of x_0 . The cost of this decomposition is a second term in the approximation error (analogous to the second term on the right-hand side of (4.8)),

$$[K_{\epsilon} * \mu](x_0) - \rho(x_0) = \int_{\mathbb{R}} K_{\epsilon}(y) (\rho_1(x_0 - y) - \rho_1(x_0)) \, dy + \int_{\mathbb{R}} K_{\epsilon}(x_0 - y) \, d\mu^{(r)}(y),$$

where $d\mu^{(r)}(y) = d\mu(y) - \rho_1(y)dy$. To ensure that this additional term does not dominate as $\epsilon \downarrow 0$, it is necessary that the kernel K(y) decays at an appropriate rate as $|y| \to \infty$. This ensures that $K_{\epsilon}(x_0 - y)$ is sufficiently small on the support of $d\mu^{(r)}(y)$ (see (4.9) for the decay in the Poisson kernel). Motivated by this discussion, we make the following definition (similar to [115, Def. 1.3]).

DEFINITION 5.1 (mth-order kernel). Let m be a positive integer and $K \in L^1(\mathbb{R})$. We say K is an mth-order kernel if it satisfies the following properties:

- (i) Normalized: $\int_{\mathbb{R}} K(x)dx = 1$.
- (ii) Zero moments: $K(x)x^j$ is integrable and $\int_{\mathbb{R}} K(x)x^j dx = 0$ for 0 < j < m.
- (iii) Decay at $\pm \infty$: There is a constant C_K , independent of x, such that

(5.1)
$$|K(x)| \le \frac{C_K}{(1+|x|)^{m+1}}, \quad x \in \mathbb{R}.$$

It is straightforward to verify that the Poisson kernel is a first-order kernel and the Gaussian kernel, i.e., $h(x) = (2\pi)^{-1/2}e^{-x^2/2}$, is a second-order kernel. While the Gaussian kernel plays an important role in DOS calculations [70] and kernel density estimation [93], it is not as useful in our framework since the evaluation of $h_{\epsilon} * \mu_f$ is not immediately related to pointwise evaluations of the resolvent (see subsection 5.1).

Since an *m*th-order kernel, K, is an approximation to the identity, one can show that $K_{\epsilon} * \mu_f$ converges weakly to μ_f . Moreover, in intervals where μ_f is absolutely continuous and sufficiently regular, $K_{\epsilon} * \mu_f$ converges pointwise to ρ_f and the rate of convergence increases with the smoothness of ρ_f , up to a maximum of $\mathcal{O}(\epsilon^m \log(1/\epsilon))$.

THEOREM 5.2. Let K be an mth-order kernel and suppose that the measure μ_f is absolutely continuous on $I=(x_0-\eta,x_0+\eta)$ for $\eta>0$ and a fixed $x_0\in\mathbb{R}$. Let ρ_f be the Radon-Nikodym derivative of the absolutely continuous component of μ_f , and suppose that $\rho_f\in\mathcal{C}^{n,\alpha}(I)$ with $\alpha\in[0,1)$. Denote the pointwise error by $E_\epsilon(x)=|\rho_f(x)-[K_\epsilon*\mu_f](x)|$. Then the following hold:

(i) If $n + \alpha < m$, then, for a constant $C(n, \alpha)$ depending only on n and α , (5.2)

$$E_{\epsilon}(x_0) \leq \frac{C_K \epsilon^m}{(\epsilon + \frac{\eta}{2})^{m+1}} + C(n, \alpha) \|\rho_f\|_{\mathcal{C}^{n, \alpha}(I)} \int_{\mathbb{R}} |K(y)| |y|^{n+\alpha} dy (1 + \eta^{-n-\alpha}) \epsilon^{n+\alpha}.$$

(ii) If $n + \alpha \ge m$, then, for a constant C(m) depending only on m, (5.3)

$$E_{\epsilon}(x_0) \leq \frac{C_K \epsilon^m}{(\epsilon + \frac{\eta}{2})^{m+1}} + C(m) \|\rho_f\|_{\mathcal{C}^m(I)} \left(C_K + \int_{-\frac{\eta}{\epsilon}}^{\frac{\eta}{\epsilon}} |K(y)| |y|^m dy \right) (1 + \eta^{-m}) \epsilon^m.$$

Here, C_K is from (5.1).

Using (5.1) to bound |K(y)| in (5.2) and (5.3), Theorem 5.2 shows that, under local regularity conditions near $x_0 \in \mathbb{R}$ and for fixed $\eta > 0$, an mth-order kernel has

$$|\rho_f(x_0) - [K_{\epsilon} * \mu_f](x_0)| = \mathcal{O}(\epsilon^{n+\alpha}) + \mathcal{O}(\epsilon^m \log(1/\epsilon))$$
 as $\epsilon \downarrow 0$.

The logarithmic term appears in the case that $K(x)x^m$ is not integrable. The upper bounds on $E_{\epsilon}(x_0)$ in Theorem 5.2 deteriorate as the interval of regularity shrinks $(\eta \to 0)$, which is to be expected.⁸

5.1. Rational Kernels. Now that we know the necessary properties of a kernel K such that $K_{\epsilon} * \mu_f$ achieves high-order convergence (see Definition 5.1), we can develop a resolvent-based approach to approximately evaluate a spectral measure more efficiently. The key to our computational framework (see section 4) is the connection between the smoothed measure and the resolvent in (4.3). This relationship allows us to compute the convolution of the measure μ_f with the Poisson kernel by evaluating the resolvent operator at the poles of the (rescaled) Poisson kernel. In other words, we can sample the smoothed measure by solving the shifted linear equations in (4.6).

Using the identity in (4.2), we can build generalizations of (4.3) for convolutions with rational functions. Suppose that the kernel K is of the form

(5.4)
$$K(x) = \frac{1}{2\pi i} \sum_{j=1}^{n_1} \frac{\alpha_j}{x - a_j} - \frac{1}{2\pi i} \sum_{j=1}^{n_2} \frac{\beta_j}{x - b_j},$$

where a_1, \ldots, a_{n_1} are distinct points in the upper half-plane and b_1, \ldots, b_{n_2} are distinct points in the lower half-plane. We restrict K to having only simple poles to avoid the need to compute powers of the resolvent. Using (4.2), the convolution $K_{\epsilon} * \mu_f$ is given by

$$(5.5) [K_{\epsilon} * \mu_f](x) = \frac{-1}{2\pi i} \left[\sum_{j=1}^{n_1} \alpha_j \langle \mathcal{R}_{\mathcal{L}}(x - \epsilon a_j) f, f \rangle - \sum_{j=1}^{n_2} \beta_j \langle \mathcal{R}_{\mathcal{L}}(x - \epsilon b_j) f, f \rangle \right].$$

Our goal is to choose the poles and residues in (5.4) so that K is an mth-order kernel. Given an integer $m \ge 1$, we are interested in finding the smallest possible n_1 and n_2 in (5.4) so that (5.5) is as efficient to evaluate as possible.

We want $K(x) = \mathcal{O}(|x|^{-(m+1)})$ as $|x| \to \infty$, which forces linear constraints to hold between the $\alpha_1, \ldots, \alpha_{n_2}$ and $\beta_1, \ldots, \beta_{n_2}$ parameters, as follows. Generically, K in (5.4) is a type (n_1+n_2-1, n_1+n_2) rational function, which means it can be written as the quotient of a degree $n_1 + n_2 - 1$ polynomial and a degree $n_1 + n_2$ polynomial.

⁸Similar results to Theorem 5.2, without the first term on the right-hand sides of (5.2) and (5.3), for absolutely continuous probability measures with globally Hölder continuous density functions are used in kernel density estimation in statistics (see, for example, [115, Prop. 1.2]).

In this form, the coefficient of highest power of x in the numerator is a multiple of

$$\sum_{j=1}^{n_1} \alpha_j - \sum_{j=1}^{n_2} \beta_j,$$

which must vanish for K to have sufficient decay. Under this condition, we find that

$$K(x)x = \frac{1}{2\pi i} \sum_{j=1}^{n_1} \frac{\alpha_j a_j}{x - a_j} - \frac{1}{2\pi i} \sum_{j=1}^{n_2} \frac{\beta_j b_j}{x - b_j}.$$

We can apply the same argument as before to see that when $m \geq 2$, we require that

$$\sum_{j=1}^{n_1} \alpha_j a_j - \sum_{j=1}^{n_2} \beta_j b_j = 0.$$

We repeat this process m-1 times (each time multiplying each term in the sum by the appropriate a_j or b_j) to find that $K(x) = \mathcal{O}(|x|^{-(m+1)})$ as $|x| \to \infty$ if and only if

(5.6)
$$\sum_{j=1}^{n_1} \alpha_j a_j^k = \sum_{j=1}^{n_2} \beta_j b_j^k, \qquad k = 0, \dots, m-1.$$

Assuming (5.6) is satisfied, the normalization and zero moment conditions (see properties (i) and (ii) of Definition 5.1) provide us with m linear conditions on the moments of K, which can be computed explicitly via contour integration. Employing a semicircle contour in the upper half-plane, applying Cauchy's residue theorem, and taking the radius of the semicircle to infinity, we find that the moments are given in terms of the poles and residues of K, i.e.,

$$\int_{\mathbb{R}} K(y)y^k \, dy = \sum_{j=1}^{n_1} \alpha_j a_j^k = \sum_{j=1}^{n_2} \beta_j b_j^k, \qquad k = 0, \dots, m-1,$$

where the second equality follows from (5.6) or closing the contour in the lower halfplane. Therefore, the rational kernel in (5.4) is an mth-order kernel, provided that the following (transposed) Vandermonde systems are satisfied:

$$(5.7) \qquad \begin{pmatrix} 1 & \dots & 1 \\ a_1 & \dots & a_{n_1} \\ \vdots & \ddots & \vdots \\ a_1^{m-1} & \dots & a_{n_1}^{m-1} \end{pmatrix} \begin{pmatrix} \alpha_1 \\ \alpha_2 \\ \vdots \\ \alpha_{n_1} \end{pmatrix} = \begin{pmatrix} 1 & \dots & 1 \\ b_1 & \dots & b_{n_2} \\ \vdots & \ddots & \vdots \\ b_1^{m-1} & \dots & b_{n_2}^{m-1} \end{pmatrix} \begin{pmatrix} \beta_1 \\ \beta_2 \\ \vdots \\ \beta_{n_2} \end{pmatrix} = \begin{pmatrix} 1 \\ 0 \\ \vdots \\ 0 \end{pmatrix}.$$

The systems in (5.7) are guaranteed to have solutions when $n_1, n_2 \ge m$. For computational efficiency, we select $n_1 = n_2 = m$ poles in the upper and lower half-planes. The Poisson kernel fits into this setting with m = 1, $a_1 = \overline{b_1} = i$, and $a_1 = \beta_1 = 1$.

It may appear from (5.5) that we need 2m resolvent evaluations to evaluate $K_{\epsilon}*\mu_f$ at a single point x. However, if the poles are selected so that $b_j = \overline{a_j}$ and $\beta_j = \overline{\alpha_j}$, then the conjugate symmetry of the resolvent, i.e., $\langle \mathcal{R}_{\mathcal{L}}(\bar{z})f, f \rangle = \overline{\langle \mathcal{R}_{\mathcal{L}}(z)f, f \rangle}$, reduces the number of resolvent evaluations to m. With this choice, we find that

$$[K_{\epsilon} * \mu_f](x) = \frac{-1}{\pi} \sum_{j=1}^{m} \operatorname{Im} \left(\alpha_j \left\langle \mathcal{R}_{\mathcal{L}}(x - \epsilon a_j) f, f \right\rangle \right),$$

which is analogous to (4.5). While the properties of an mth order kernel determine the number of poles and the residues of K (see (5.7)), the locations of the poles in the upper half-plane are left to our discretion.

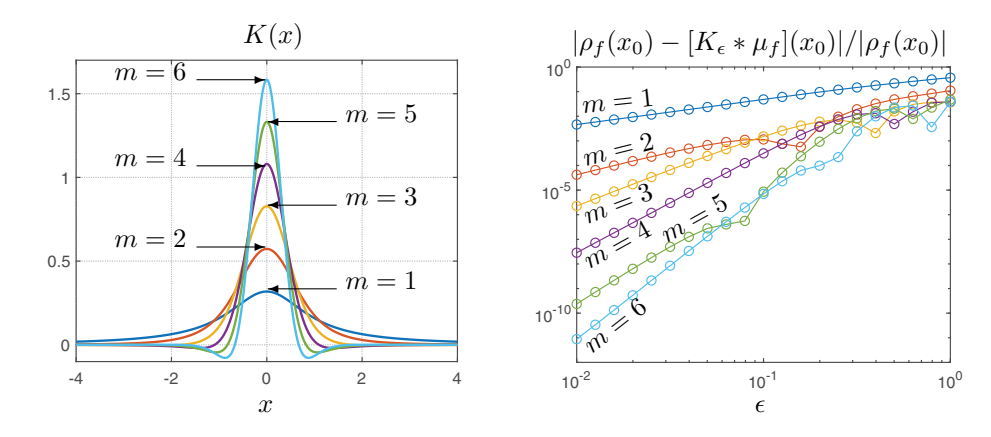


Fig. 5.1 Left: The mth-order kernels constructed from (5.7) with poles in (5.8) for $1 \le m \le 6$. Right: The pointwise relative error in smoothed measures of the integral operator in (4.7) computed using the high-order kernels with poles in (5.8) for $1 \le m \le 6$. The relative error is computed by comparing with a numerical solution that is resolved to machine precision.

Table 5.1 The numerators and residues of the first six rational kernels with equispaced poles (see (5.8)). We give the first $\lceil m/2 \rceil$ residues because the others follow by the symmetry $\alpha_{m+1-j} = \overline{\alpha_j}$.

m	$\pi K(x) \prod_{j=1}^{m} (x - a_j)(x - \overline{a_j})$	$\{\alpha_1,\ldots,\alpha_{\lceil m/2\rceil}\}$
2	$\frac{20}{9}$	$\left\{\frac{1+3i}{2}\right\}$
3	$-\frac{5}{4}x^2 + \frac{65}{16}$	$\{-2+i,5\}$
4	$-\frac{3536}{625}x^2 + \frac{21216}{3125}$	$\left\{\frac{-39-65i}{24}, \frac{17+85i}{8}\right\}$
5	$\frac{130}{81}x^4 - \frac{12350}{729}x^2 + \frac{70720}{6561}$	$\left\{\frac{15-10i}{4}, \frac{-39+13i}{2}, \frac{65}{2}\right\}$
6	$\frac{1287600}{117649}x^4 - \frac{34336000}{823543}x^2 + \frac{667835200}{40353607}$	$\left\{\frac{725+1015i}{192}, \frac{-2775-6475i}{192}, \frac{1073+7511i}{96}\right\}$

5.1.1. Equispaced Poles. As a natural extension of the Poisson kernel, whose two poles are at $\pm i$, we consider the family of mth-order kernels with equispaced poles in the upper and lower half-planes given by

(5.8)
$$a_j = \frac{2j}{m+1} - 1 + i, \quad b_j = \overline{a_j}, \quad 1 \le j \le m.$$

We then determine the residues by solving the Vandermonde system in (5.7). The first six kernels are plotted in Figure 5.1 (left) and are explicitly written down in Table 5.1.

Empirically, we have found that the choice in (5.8) performs slightly better than other natural choices such as Chebyshev points with an offset +i, rotated roots of unity, or dyadic poles $a_j = i2^{-j}$. Dyadic poles have the advantage that if ϵ is halved, the resolvent only needs to be computed at one additional point. The ill-conditioning of the Vandermonde system does not play a role for the values of m here. Moreover, equispaced poles are particularly useful when one wishes to sample the smoothed measure $K_{\epsilon} * \mu_f$ over an interval since samples of the resolvent can be reused for different points in the interval. Finally, if ϵ is found to be insufficiently small, instead

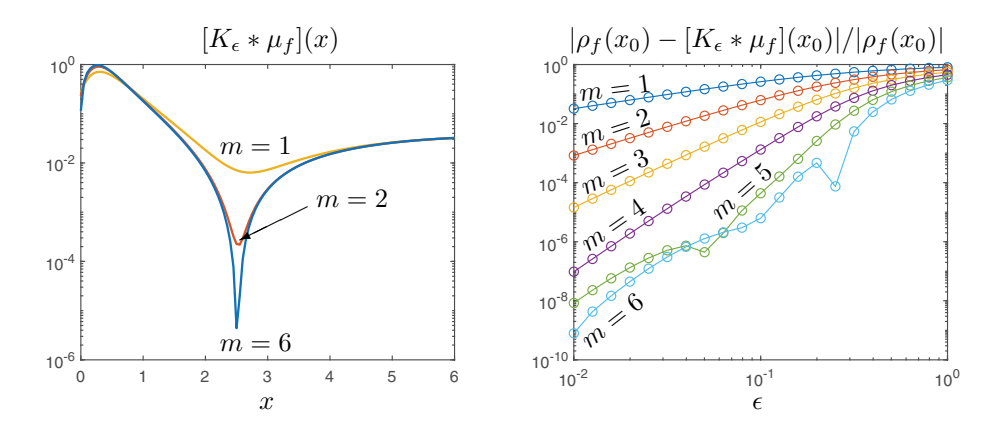


Fig. 5.2 Results for the Schrödinger operator in (4.11) using mth-order kernels with equispaced poles (see (5.8)). Left: Smoothed approximations to the spectral measure. Right: Pointwise relative error, computed by comparing with a numerical solution resolved to machine precision.

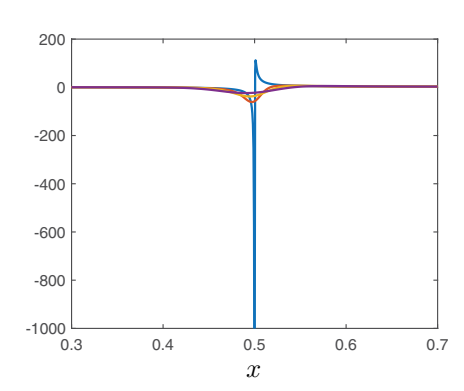
of reevaluating the resolvent at m points, one can add poles closer to the real axis (with a smaller ϵ) and reuse the old resolvent evaluations. This effectively increases m, and hence the coefficients α_j need to be recomputed. This may be computationally beneficial since the cost of solving the Vandermonde system is typically negligible compared to the cost of evaluating the resolvent close to the real axis.

To demonstrate the practical advantage of high-order kernels, we revisit the examples from section 4 and compute the smoothed measure $K_{\epsilon} * \mu_f$ using mth-order kernels with equispaced poles. In Figure 5.1 (right) and Figure 5.2 (right), we observe the convergence rates predicted in Theorem 5.2 for the integral operator in (4.7) and the differential operator in (4.11), respectively. While the Poisson kernel requires us to solve linear equations with shifts extremely close to the continuous spectrum to achieve a few digits of accuracy in our approximation to ρ_f , a sixth-order kernel enables us to achieve about 11 and 9 digits of accuracy, respectively, without decreasing ϵ below 0.01. Figure 5.2 (left) shows the increased resolution obtained when using high-order kernels for the differential operator in (4.11) with smoothing parameter $\epsilon = 0.1$. Although using a sixth-order kernel requires six times as many resolvent evaluations as that of the Poisson kernel, this is typically favorable because the cost of evaluating the resolvent near the continuous spectrum of \mathcal{L} increases as $\epsilon \downarrow 0$ (see subsection 4.3).

In Figure 5.3 (which should be compared to Figure 4.2), we plot the real part of the linear combination of solutions, given by

$$\operatorname{Re}\left(\sum_{j=1}^{m}\beta_{j}\mathcal{R}_{\mathcal{L}}(x-\epsilon b_{j})f\right).$$

Here, ϵ is selected to achieve a relative error of 0.0001 and 0.005 in the density of the integral and Schrödinger operators, respectively. For a fixed relative error, the high-order kernels lead to numerical solutions that are less peaked (or less oscillatory), which allows us to use much smaller discretizations of the linear operators.



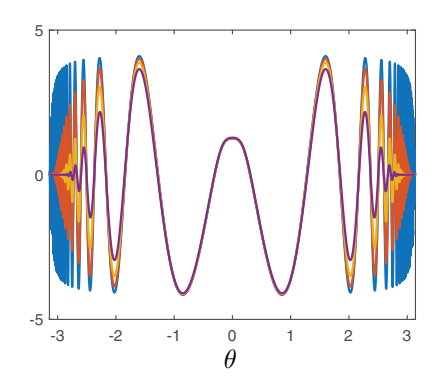


Fig. 5.3 Real part of $\sum_{j=1}^{m} \beta_j \mathcal{R}_{\mathcal{L}}(x - \epsilon b_j) f$, where ϵ is chosen to achieve a relative error of 0.0001 for the integral operator in (4.7) (left) and 0.005 for the Schrödinger operator in (4.11) (right), with m=1 (blue), m=2 (yellow), m=3 (orange), and m=4 (purple). Recall that the solutions to (4.11) are mapped to $[-\pi, \pi]$ via $x=10i(1-e^{i\theta})/(1+e^{i\theta})$.

5.2. Other Types of Convergence. Consider the radial Schrödinger operator with a Hellmann potential and angular momentum quantum number ℓ , given by [51]

(5.9)
$$[\mathcal{L}u](r) = -\frac{d^2u}{dr^2}(r) + \left(\frac{\ell(\ell+1)}{r^2} + \frac{1}{r}(e^{-r} - 1)\right)u(r), \qquad r > 0.$$

The spectral properties of \mathcal{L} are of interest in quantum chemistry, where the Hellman potential models atomic and molecular ionization processes [49]. Ionization rates and related transition probabilities are usually studied by computing bound and resonant states of \mathcal{L} ; however, we compute this information directly from the spectral measure.

For example, if $f(r) = Ce^{-(r-r_0)^2}$ (where C is chosen so that $||f||_{L^2(\mathbb{R}_+)} = 1$) is the radial component of the wave function of an electron interacting with an atomic core via the Hellmann potential in (5.9), then we can calculate the probability that the electron escapes from the atomic core with energy $E \in [a, b]$ (with 0 < a < b) via

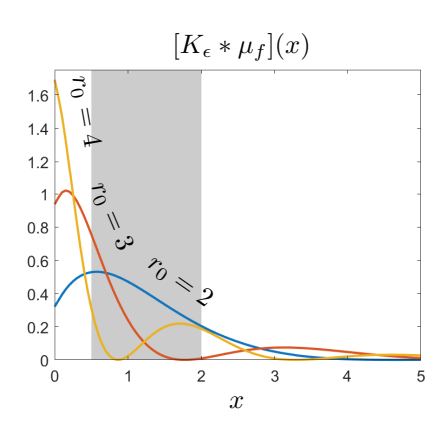
(5.10)
$$\mathbb{P}(a \le E \le b) = \mu_f([a, b]) \approx \int_a^b [K_\epsilon * \mu_f](y) \, dy, \qquad \epsilon \ll 1.$$

The error for the approximation in (5.10) is bounded above by

$$\left| \mu_f([a,b]) - \int_a^b \left[K_{\epsilon} * \mu_f \right](y) \, dy \right| \le \int_a^b \left| \rho_f(y) - \left[K_{\epsilon} * \mu_f \right](y) \right| \, dy = \| \rho_f - K_{\epsilon} * \mu_f \|_{L^1([a,b])}.$$

This leads us naturally to the notion of L^p convergence on an interval. The smoothed measure always converges to ρ_f in $L^1([a,b])$ when μ_f is absolutely continuous on [a,b]. However, in analogy with the pointwise results in subsection 4.2 and section 5, we need to impose some additional regularity on ρ_f to obtain rates of convergence. We let $\mathcal{W}^{k,p}(I)$ denote the Sobolev space of functions in $L^p(I)$ such that f and its weak derivatives up to order k have a finite L^p norm [37].

THEOREM 5.3. Let K be an mth-order kernel and $1 \le p < \infty$. Suppose that the measure μ_f is absolutely continuous on the interval $I = (a - \eta, b + \eta)$ for $\eta > 0$ and some a < b. Let ρ_f denote the Radon-Nikodym derivative of the absolutely continuous



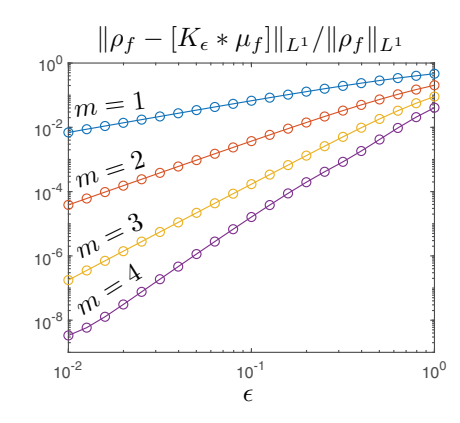


Fig. 5.4 Left: The smoothed approximation to the density on the absolutely continuous spectrum of \mathcal{L} in (5.9), with $f_{r_0}(r) = C_{r_0}e^{-(r-r_0)^2}$ and $\ell=1$, for $r_0=2$, $r_0=3$, and $r_0=4$ (C_{r_0} is a normalization constant so that $||f_{r_0}||_{L^2(\mathbb{R}_+)}=1$). The shaded area under each curve corresponds to $\mathbb{P}(1/2 \leq E \leq 2)$ in (5.10) for the particle with wave function $f_{r_0}(r)$. Right: The $L^1((1/2,2))$ relative error in smoothed measures for the radial Schrödinger operator in (5.9). The relative error is computed by comparing with a numerical solution that is resolved to machine precision.

component of μ_f , and suppose that $\rho_I := \rho_f|_I \in \mathcal{W}^{m,p}(I)$. Then

$$\|\rho_{I} - [K_{\epsilon} * \mu_{f}]\|_{L^{p}((a,b))} \leq \frac{C_{K}(b-a)^{1/p}}{\left(\epsilon + \frac{\eta}{2}\right)^{m+1}} \epsilon^{m} + C(m)C_{K}\|\rho_{I}\|_{\mathcal{W}^{k,p}(I)} \left(1 + \eta^{-m}\right) \log\left(1 + \frac{b-a+2\eta}{\epsilon}\right) \epsilon^{m},$$

where C(m) is a constant depending only on m, and C_K is from (5.1).

Proof. See Appendix A.2.
$$\Box$$

Theorem 5.3 implies the asymptotic error rate⁹

$$\|\rho_I - [K_{\epsilon} * \mu_f]\|_{L^p(I)} = \mathcal{O}(\epsilon^m \log(1/\epsilon))$$
 as $\epsilon \downarrow 0$.

The L^1 convergence for the approximation to the probabilities in (5.10) is shown in Figure 5.4 (right), which agrees with the asymptotic rates implied by Theorem 5.3.

If one wishes to compute dynamics of the electron interacting with the atomic core via the Hellman potential, then we need a slightly weaker form of convergence. For instance, the time autocorrelation of the electron's wave function can be computed by integrating the function $F_t(E) = e^{-iEt}$ against the measure μ_f , so that

$$\mu_f(F_t) = \langle e^{-i\mathcal{L}t}f, f\rangle = \int_{-\infty}^{\infty} e^{-iyt} \, d\mu_f(y) \approx \int_{-\infty}^{\infty} e^{-iyt} \, [K_{\epsilon} * \mu_f](y) \, dy, \quad \epsilon \ll 1.$$

Unlike the previous cases of pointwise and L^1 convergence, we do not need any additional requirements on the measure μ_f , which may be singular and have discrete

⁹Theorem 5.3 for p=2 without the first term on the right-hand side and for absolutely continuous probability measures with $\mathcal{W}^{m,2}(\mathbb{R})$ density function is used in kernel density estimation in statistics [115, Prop. 1.5]. In this context, the L^2 error is used to bound the bias term in the mean integrated squared error. The case of L^1 convergence requires a different proof technique.

components, to obtain convergence rates. Instead, we require that the function F be sufficiently smooth. For example, if $F \in \mathcal{C}^{n,\alpha}(\mathbb{R})$ and K is an mth-order kernel, then approximating F via convolutions and applying Fubini's theorem shows that

$$|\mu_f(F) - [K_{\epsilon} * \mu_f](F)| = \mathcal{O}(\epsilon^{n+\alpha}) + \mathcal{O}(\epsilon^m \log(1/\epsilon))$$
 as $\epsilon \downarrow 0$.

Finally, note that a kernel cannot be nonnegative everywhere and have an order greater than two. This is not a problem in practice since we can replace $[K_{\epsilon} * \mu_f](x)$ by $\max\{0, [K_{\epsilon} * \mu_f](x)\}$ with the same error bounds in Theorems 5.2 and 5.3.

6. The Resolvent Framework in Practice. Given an mth-order rational kernel, defined by distinct poles a_1, \ldots, a_m in the upper half-plane, the resolvent-based framework for evaluating an approximate spectral measure is summarized in Algorithm 6.1. This algorithm, which can be performed in parallel for several x_0 , forms the foundation of SpecSolve. SpecSolve uses equispaced poles (see subsection 5.1.1) by default, but users may select other options with the name-value pair 'PoleType'.

Algorithm 6.1 A practical framework for evaluating an approximate spectral measure of an operator \mathcal{L} at $x_0 \in \mathbb{R}$ with respect to a vector $f \in \mathcal{H}$.

Input: $\mathcal{L}: \mathcal{D}(\mathcal{L}) \to \mathcal{H}, f \in \mathcal{H}, x_0 \in \mathbb{R}, a_1, \dots, a_m \in \{z \in \mathbb{C}: \text{Im}(z) > 0\}, \text{ and } \epsilon > 0.$

- 1: Solve the Vandermonde system (5.7) for the residues $\alpha_1, \ldots, \alpha_m \in \mathbb{C}$.
- 2: Solve $(\mathcal{L} (x_0 \epsilon a_j))u_i^{\epsilon} = f$ for $1 \leq j \leq m$.
- 3: Compute $\mu_f^{\epsilon}(x_0) = \frac{-1}{\pi} \operatorname{Im} \left(\sum_{j=1}^m \alpha_j \langle u_j^{\epsilon}, f \rangle \right)$.

Output: $\mu_f^{\epsilon}(x_0)$.

In practice, the resolvent in Algorithm 6.1 is discretized before being applied. We compute an accurate value of μ_f^{ϵ} , provided that the resolvent is applied with sufficient accuracy (see Figure 4.1), which can be done adaptively with a posteriori error bounds [16]. For an efficient adaptive implementation, SpecSolve constructs a fixed discretization, solves linear systems at each required complex shift, and checks the approximation error at each shift. If further accuracy is needed at a subset of the shifts, then the discretization is refined geometrically, applied at these shifts, and the error is recomputed. This process is repeated until the resolvent is computed accurately at all shifts. The user may (optionally) specify initial and maximum discretization sizes with the name-value pairs 'DiscMin' and 'DiscMax'.

SpecSolve supports three types of operators: (1) ordinary differential operators, (2) integral operators, and (3) infinite matrices with finitely many nonzeros per column. For more general operators and inner products, the user must supply a command that solves the shifted linear equations in Algorithm 6.1 and a command that evaluates the inner products, allowing a user to evaluate spectral measures for exotic problems and employ their favorite discretization.

6.1. Ordinary Differential Operators. As part of its capabilities, SpecSolve computes samples from a smoothed approximation to the spectral measure of a self-adjoint, regular ordinary differential operator on the real line or on the half line, i.e.,

(6.1)
$$[\mathcal{L}u](x) = c_p(x) \frac{d^p u}{dx^p}(x) + \dots + c_1(x) \frac{du}{dx}(x) + c_0(x)u(x), \qquad p \ge 0.$$

with the standard inner products. Here, the variable coefficients c_0, \ldots, c_p are smooth functions and $c_p \neq 0$ on the relevant domain (real line or half line). Note that \mathcal{L} in (6.1)

is not necessarily self-adjoint: the user provides the variable coefficients c_0, \ldots, c_p and must verify that \mathcal{L} is self-adjoint.

To demonstrate, recall the Schrödinger operator defined on the real line in (4.11). We can compute a smoothed approximation to its spectral measure using the function diffMeas as follows:

The differential operator is specified by its coefficients c_0, \ldots, c_2 , which are input as a cell array of function handles. Given evaluation points xi and function handle f, diffMeas computes the smoothed measure, with respect to f, using the specified smoothing parameter and kernel order (the default kernel is m = 2).

To apply the resolvent of a differential operator acting on functions on the real line, the associated differential equation (see Algorithm 6.1) is automatically transplanted to the periodic interval $[-\pi,\pi]$ with an analytic map and solved with an adaptive Fourier spectral method [9]. Typically, the differential equation has singular points at $\pm \pi$ after mapping, and the Fourier spectral method usually converges to a bounded analytic solution [9, sect. 17.8]. Similarly, on the half line, the differential equation is mapped to the unit interval [-1,1] with an analytic map and solved with an adaptive nonperiodic analogue of the Fourier spectral method known as the ultraspherical spectral method [77]. After solving the differential equation on the mapped domain, the inner products in (4.5) are computed using a trapezoidal rule (for the unit circle) [113] or a Clenshaw-Curtis rule (for the unit interval) [111, Chap. 19].

In many applications, differential operators on the half line may have a singular point at the origin. This makes an efficient and automatic representation of variable coefficients somewhat subtle. For example, the radial Schrödinger operator in (5.9) has a singular point at the origin for $\ell \geq 1$, and the shifted linear equations in Algorithm 6.1 should be multiplied through by r^2 so that subsequent discretizations yield sparse, banded matrices [77]. In addition to diffMeas, SpecSolve contains a small gallery of functions that sample smoothed spectral measures for common operators with singular points, such as rseMeas, which samples the smoothed measure of the radial Schrödinger operator with a user-specified potential.

To illustrate, we use rseMeas to compute $\mathbb{P}(1/2 \le E \le 2)$ from (5.10):

The user specifies the potential of the radial Schrödinger operator through a cell array of function handles: $V\{1\}$ is the nonsingular part of the potential, $V\{2\}$ is the variable coefficient for the r^{-1} Coulomb term, and $V\{3\}$ is the quantum angular momentum number that defines the coefficient for the r^{-2} centrifugal term.

6.2. Integral Operators. In SpecSolve, the function intMeas computes samples from a smoothed approximation of the spectral measure of an integral operator, acting

on functions defined on [-1, 1], of the form

$$[\mathcal{L}u](x) = a(x)u(x) + \int_{-1}^{1} g(x,y) u(y) dy, \qquad x \in [-1,1], \qquad u \in L^{2}([-1,1]).$$

We assume that the multiplicative coefficient a(x) and the kernel g(x,y) are smooth functions (well approximated by polynomials) and that g(x,y) = g(y,x) so that \mathcal{L} is self-adjoint with respect to the standard inner product. Revisiting the integral operator from (4.7), we can compute the smoothed measure with a few simple commands:

The integral operator is specified by a cell array containing function handles for the kernel and multiplicative coefficient. Given smoothing parameter and kernel order, the smoothed measure is approximated at the evaluation points \mathtt{xi} .

To apply the resolvent, we use an adaptive Chebyshev collocation scheme to solve the shifted linear systems in Algorithm 6.1. For efficient storage and computation, we exploit low numerical rank structure in the discretization of the smooth kernels when possible [110]. We apply a Clenshaw–Curtis quadrature rule to compute the inner products required to sample μ_f^{ϵ} [111].

6.3. Infinite Sparse Matrices. In SpecSolve, the function infmatMeas deals with discrete systems. We consider the canonical Hilbert space $\ell^2(\mathbb{N})$ (with the standard inner product) and assume that \mathcal{L} is realized as an infinite matrix A such that

$$A = \begin{pmatrix} a_{11} & a_{12} & \dots \\ a_{21} & a_{22} & \dots \\ \vdots & \vdots & \ddots \end{pmatrix}, \qquad a_{ij} = \langle \mathcal{L}e_j, e_i \rangle = \overline{a_{ji}},$$

where e_i is the *i*th canonical unit vector. We assume that the span of the canonical basis forms a core^{10} of \mathcal{L} and that there is a known function $F: \mathbb{N} \to \mathbb{N}$ such that $a_{ij} = 0$ if i > F(j).¹¹ There is no loss of generality in working in $\ell^2(\mathbb{N})$ since we can always choose an orthonormal basis of a separable Hilbert space to obtain $\mathcal{H} \cong \ell^2(\mathbb{N})$. The majority of graph operators that are encountered in physics can be put into this framework. For example, given a finite range interaction Hamiltonian on $\ell^2(\mathbb{Z}^d)$, one can enumerate the vertices of the graph to obtain a realization of $\ell^2(\mathbb{Z}^d) \cong \ell^2(\mathbb{N})$ as well as an associated function F. The value of $[K_{\epsilon} * \mu_f](x_0)$ for some $f \in \ell^2(\mathbb{N})$ is then approximated through least-squares solutions of the rectangular systems [16]

$$P_{F(N)}(A - (x_0 + \epsilon a_j))P_N u_j^{\epsilon} = P_{F(N)}f,$$

where P_n denotes the orthogonal projection onto the span of the first n basis vectors. For a rectangular truncation $H = P_{F(N)}AP_N$ supplied by the user, we can, for example, compute the smoothed measure with respect to the first canonical basis vector via the following commands:

¹⁰This technical condition means that the closure of \mathcal{L} restricted to the span of the canonical basis is \mathcal{L} , and hence we can equate \mathcal{L} with the infinite matrix A.

 $^{^{11}}$ Weaker assumptions such as known asymptotic decay of each column are also possible.

An example for a magnetic Schrödinger equation on a graphene lattice (see subsection 7.2) is provided in the gallery of examples in SpecSolve.

- **7. Examples.** We now provide three examples to demonstrate the versatility of our computational framework.
- **7.1. Example 1: Beam and Two-Dimensional Schrödinger Equations.** The increased computational efficiency achieved through high-order kernels allows us to treat PDEs and high-order ODEs. First, consider a fourth-order differential operator associated with the elastic beam equation given by

$$(7.1) [\mathcal{L}u](x) = \frac{d^4u}{dx^4}(x) - \frac{d}{dx} \left[\left(1 - e^{-x^2} \right) \frac{du}{dx} \right](x) + \frac{a\sin(x)}{1 + x^2} u(x), x \in \mathbb{R}$$

for some constant $a \in \mathbb{R}$. Figure 7.1 (left) shows $K_{\epsilon} * \mu_f$ for a second-order kernel with $\epsilon = 0.05$ and $f(x) = \sqrt{2\pi^{-1}}/(1+x^2)$, when a = 0, 5, and 10. When a = 0, the operator is positive with continuous spectrum in $[0, \infty)$. When $a \neq 0$, there is also an eigenvalue below the continuous spectrum, corresponding to the spikes in Figure 7.1 (left). We also observe that different values of a alter the profile of ρ_f on $[0, \infty)$.

Next, consider the two-dimensional Schrödinger operator given by (7.2)

$$[\mathcal{L}u](x_1, x_2) = -\nabla^2 u(x_1, x_2) + \left(\frac{e^{-x_1^2}}{1 + x_2^2} + a\left(\operatorname{erf}(x_1) + \operatorname{erf}(x_2)\right)\right) u(x_1, x_2), \quad x_j \in \mathbb{R},$$

for some constant $a \in \mathbb{R}$, where $\operatorname{erf}(\cdot)$ is the error function. To apply the resolvent we map \mathbb{R}^2 to the torus $[-\pi,\pi]^2$ via $x_j \to 10i(1-e^{i\theta_j})/(1+e^{i\theta_j})$. We then use a tensorized Fourier spectral method with hyperbolic cross ordering of the basis functions [72, Chap. III]. Figure 7.1 (right) shows $K_{\epsilon} * \mu_f$ for a fourth-order kernel with $\epsilon = 0.2$ and $f(x_1,x_2) = \exp(-x_1^2 - x_2^2)\sqrt{2\pi^{-1}}$, when a = 0,1, and 2. The spectrum of the operator is $[-2a,\infty)$, and we observe that the convolution $[K_{\epsilon} * \mu_f](x)$ takes small negative values in the vicinity of the lower boundary of the spectrum.

- **7.2. Example 2: The Schrödinger Equation on a Graphene Lattice.** We now apply our method to a magnetic tight-binding model of graphene, which involves a discrete graph operator [1]. Graphene is a two-dimensional material with carbon atoms situated at the vertices of a honeycomb lattice (see Figure 7.2), whose unusual properties are studied in condensed-matter physics [11, 76]. The magnetic properties of graphene are important because of the experimental observation of the quantum Hall effect and Hofstadter's butterfly [82], and the exciting new area of twistronics [12, 71].
- **7.2.1. The Model.** A honeycomb lattice can be decomposed into two bipartite sublattices (see Figure 7.2 (left)), and thus the wave function of an electron can be modeled as the spinor [1]

$$\psi_{m,n} = (\psi_{m,n}^{[1]}, \psi_{m,n}^{[2]})^T \in \mathbb{C}^2, \qquad \psi = (\psi_{m,n}) \in l^2(\mathbb{Z}^2; \mathbb{C}^2) \cong \ell^2(\mathbb{N}).$$

Here, $(m, n) \in \mathbb{Z}^2$ labels a position on the sublattices and $\ell^2(\mathbb{Z}^2; \mathbb{C}^2)$ denotes the space of square summable \mathbb{C}^2 -valued sequences indexed by \mathbb{Z}^2 . To define the Hamiltonian,

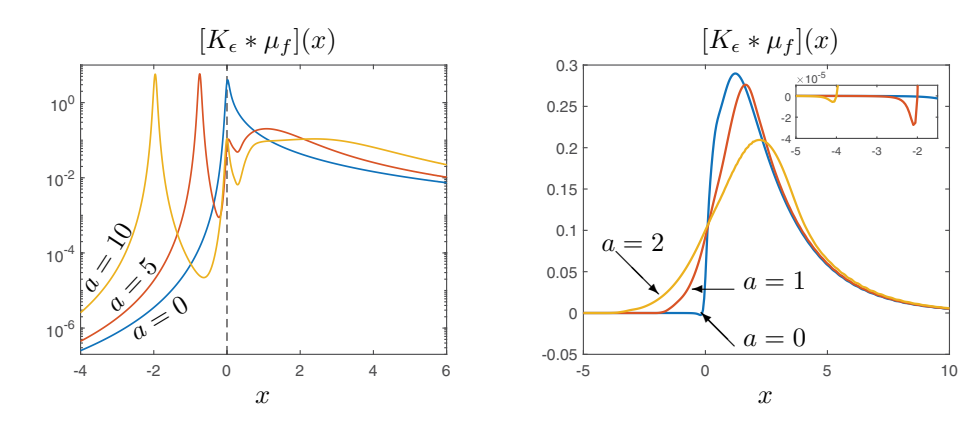


Fig. 7.1 Left: Smoothed approximations to the spectral measures of the elastic beam operators in (7.1) for a second-order kernel with a=0,5, and 10. Right: Smoothed approximations to the spectral measures of the two-dimensional Schrödinger operators in (7.2) for a fourth-order kernel with a=0,1, and 2. The magnified region demonstrates that $[K_{\epsilon}*\mu_f](x)$ is not always positive for kernels of order greater than two.

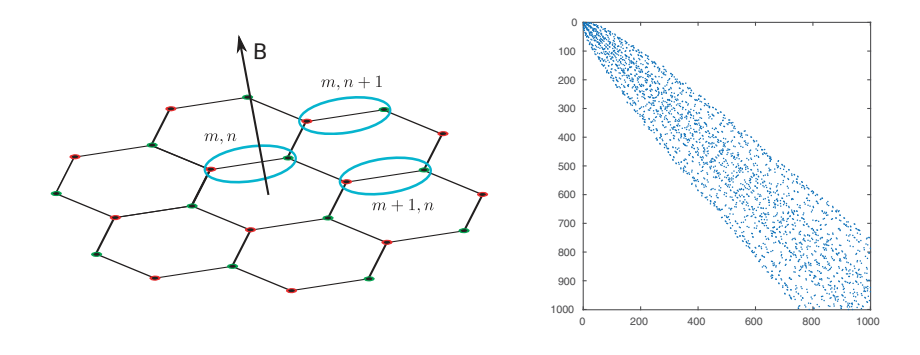


Fig. 7.2 Left: Honeycomb structure of graphene as a bipartite graph. We have shown the spinor structure via the circled lattice vertices and the indexing via (m,n). The arrow shows the perpendicular magnetic field B. Right: Sparsity structure of the first $10^3 \times 10^3$ block of the infinite matrix and the corresponding growing local bandwidth.

consider the following three magnetic hopping operators $T_1, T_2, T_3 : \ell^2(\mathbb{Z}^2; \mathbb{C}^2) \to \ell^2(\mathbb{Z}^2; \mathbb{C}^2)$ for a given magnetic flux per unit cell Φ (in dimensionless units):

$$(T_1\psi)_{m,n} = \begin{pmatrix} \psi_{m,n}^{[2]} \\ \psi_{m,n}^{[1]} \end{pmatrix}, \quad (T_2\psi)_{m,n} = \begin{pmatrix} \psi_{m+1,n}^{[2]} \\ \psi_{m-1,n}^{[1]} \end{pmatrix}, \quad (T_3\psi)_{m,n} = \begin{pmatrix} e^{-2\pi i \Phi m} \psi_{m,n+1}^{[2]} \\ e^{2\pi i \Phi m} \psi_{m,n-1}^{[1]} \end{pmatrix}.$$

After a suitable gauge transformation, the free Hamiltonian can be expressed as $H_0 = T_1 + T_2 + T_3$ and $\Lambda(H_0) \subset [-3,3]$. A suitable ordering of lattice points leads to a sparse discretization of H_0 , where the kth column contains $\mathcal{O}(\sqrt{k})$ nonzero entries (see Figure 7.2 (right)). Therefore, for an approximation using N basis sites, the action of the resolvent can be computed in $\mathcal{O}(N^{3/2})$ operations [112].

7.2.2. The Computed Measures. Figure 7.3 shows how the spectral measure of H_0 , taken with respect to the vector e_1 , varies with Φ . For $\Phi \in \mathbb{Q}$, the spectrum is absolutely continuous, and we show the Radon–Nikodym derivative of the measure,

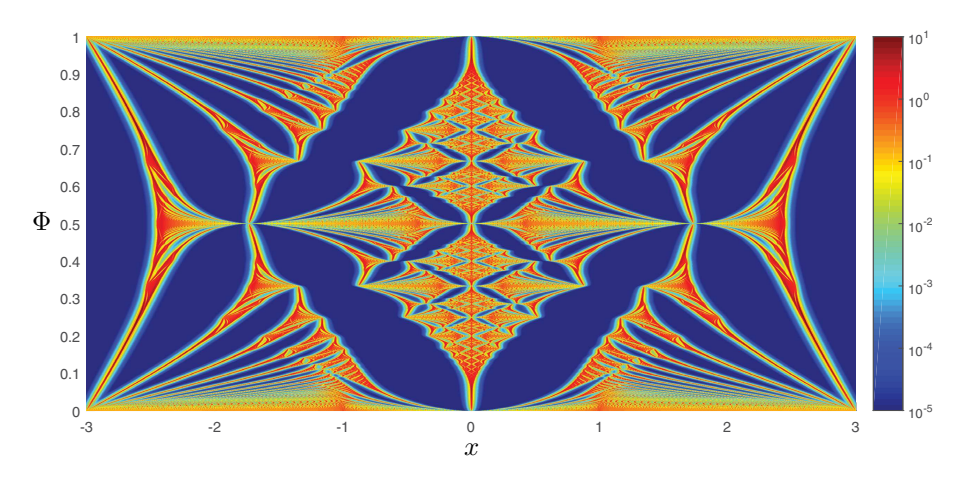


Fig. 7.3 The Radon-Nikodym derivative of the measure for various Φ , computed with $\epsilon = 0.01$. The spectrum is fractal for irrational Φ , which is approximated by rational Φ . The small gaps in the spectrum are clearly visible (corresponding to the blue shaded regions) and the logarithmic scale shows the sharpness of the approximation to ρ_{e_1} , which vanishes in these gaps.

 ρ_{e_1} . The calculations, performed with a fourth-order kernel and $\epsilon=0.01$, show a sharp Hofstadter-type butterfly.¹²

Figure 7.4 (left) shows an approximation of ρ_{e_1} when $\Phi = 1/4$ using a fourth-order kernel and $\epsilon = 0.01$. We also show, as shaded vertical strips, the output of the algorithm in [21] which computes the spectrum with error control (we use an error bound of 10^{-3}) and without spectral pollution.¹³ The support of $K_{\epsilon} * \mu_f$ is the whole real line due to the noncompact support of the kernel K. However, if $x \notin \Lambda(H_0)$, then applying (5.1) directly to the definition of convolution shows that $|[K_{\epsilon} * \mu_f](x)| \leq C_K \epsilon^m/(\epsilon + \operatorname{dist}(x, \Lambda(H_0)))^{m+1}$, where C_K is the constant in (5.1), so $|[K_{\epsilon} * \mu_f](x)|$ decays rapidly when off the spectrum. We also consider a multiplication operator (potential) perturbation, modeling a defect, of the form

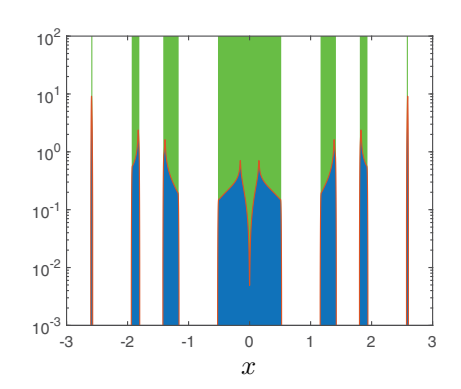
(7.3)
$$V(\mathbf{x}) = \frac{\cos(\|\mathbf{x}\|_2 \pi)}{(\|\mathbf{x}\|_2 + 1)^2},$$

where \mathbf{x} denotes the position of a vertex normalized so each edge has length 1. The perturbed operator is then H_0+V . Since the perturbation is trace class, the absolutely continuous part of the spectrum remains the same (though the measure changes) and the potential induces additional eigenvalues (see Figure 7.4 (right)). Again, we see that $|[K_{\epsilon} * \mu_f](x)|$ decays rapidly when off the spectrum. In particular, the measure is not corrupted by spikes in the gaps in the essential spectrum or similar artifacts caused by spectral pollution.

7.3. Example 3: Discrete Spectra and Dirac Operators. In this example, we consider the case of the Dirac operator $\mathcal{L} = \mathcal{D}_V$ defined below. Often this operator has discrete eigenvalues in the interval (-1,1), which forms a gap in the essential

¹²Hofstadter's butterfly [54] is the visual representation of the fractal, self-similar nature of the spectrum of a Hamiltonian describing noninteracting two-dimensional electrons in a magnetic field in a lattice. The most famous example is that of the almost Mathieu operator on $\ell^2(\mathbb{Z})$.

¹³With a nonperiodic potential (7.3), this is a highly nontrivial problem since finite truncation methods typically suffer from spectral pollution inside the convex hull of the essential spectrum.



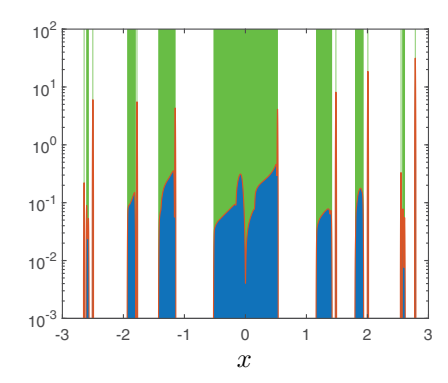


Fig. 7.4 Left: Smoothed measure with no potential. We show the algorithm in [21] as shaded strips (green) for comparison. Right: The same computation but with the added potential in (7.3).

The additional eigenvalues correspond to spikes in the smoothed measure.

spectrum. This means that standard Galerkin methods used to compute $\Lambda(\mathcal{D}_V)$ typically suffer from spectral pollution in the gap. That is, as the discretization size increases, the discrete spectrum of the Galerkin discretization clusters in a way that does not approximate $\Lambda(\mathcal{D}_V)$. There is a vast literature on methods that seek to avoid spectral pollution when computing $\Lambda(\mathcal{D}_V)$ [30, 64, 65, 91, 104]. The majority of existing approaches work for certain classes of potentials and avoid spectral pollution on particular subsets of (-1,1). Even for Coulomb-type potentials, spectral pollution can be a difficult issue to overcome, and computations typically achieve a few digits of precision for the ground state and a handful of the first few excited states. A popular approach is the so-called kinetic balance condition, which does not always work for Coulomb potentials [32, 68, 96]. Our approach does not suffer from spectral pollution and can compute the first thousand eigenvalues to near machine precision accuracy.

7.3.1. Recovering Eigenvalues and Projections onto Eigenspaces. The dominated convergence theorem applied to (4.3) shows that, for any $x \in \mathbb{R}$, we have

(7.4)
$$\lim_{\epsilon \downarrow 0} \epsilon \cdot \operatorname{Im} \left(\langle \mathcal{R}_{\mathcal{L}}(x + i\epsilon) f, f \rangle \right) = \sum_{\lambda \in \Lambda^{p}(\mathcal{L}) \cap \{x\}} \langle \mathcal{P}_{\lambda} f, f \rangle.$$

Moreover, if there is no singular continuous spectrum in a neighborhood of x, and x is not an accumulation point of $\Lambda^{p}(\mathcal{L})$, then (7.4) can be sharpened to

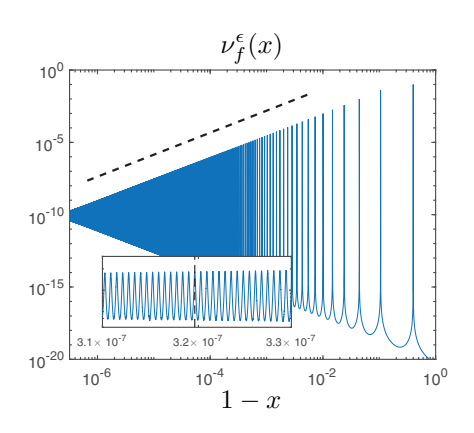
(7.5)
$$\epsilon \cdot \operatorname{Im} (\langle \mathcal{R}_{\mathcal{L}}(x+i\epsilon)f, f \rangle) = \sum_{\lambda \in \Lambda^{\mathrm{p}}(\mathcal{L}) \cap \{x\}} \langle \mathcal{P}_{\lambda}f, f \rangle + \mathcal{O}(\epsilon).$$

These formulas allow us to compute the locations of eigenvalues of the operator and the corresponding projection coefficients onto the eigenspaces for vectors f.

7.3.2. The Dirac Operator. We consider a differential operator \mathcal{D}_V associated with a coupled first-order system of differential equations that describes the motion of a relativistic spin-1/2 particle in a radially symmetric potential V(r), defined by

$$\mathcal{D}_V = \begin{pmatrix} 1 + V(r) & -\frac{d}{dr} + \frac{\kappa}{r} \\ \frac{d}{dr} + \frac{\kappa}{r} & -1 + V(r) \end{pmatrix}.$$

Here, $\kappa = j + 1/2$ for $j \in \mathbb{Z}$ (related to the angular momentum of the particle) and \mathcal{D}_V is a special case of the Dirac operator with a radially symmetric potential [107].



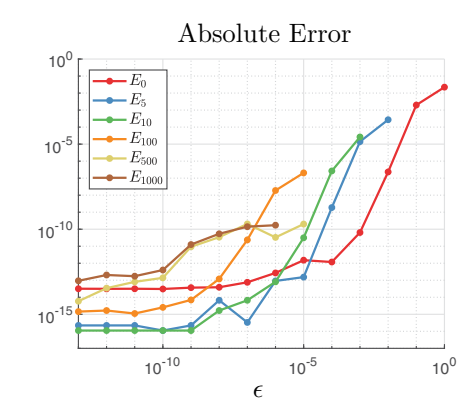


Fig. 7.5 Left: The function $\nu_f^\epsilon(x)$ for x near 1. The sloped dashed line shows the algebraic decay of $\|\mathcal{P}_{E_j}f\|^2$ (approximately $\mathcal{O}(j^{-3})$). The magnified region shows the extreme clustering, with the vertical dashed line corresponding to E_{1000} . Right: The absolute error in the computed eigenvalues $E_j(\mathcal{D}_V)$ for j=0,5,10,100,500,1000 as $\epsilon\downarrow 0$.

If V satisfies suitable conditions [107], then \mathcal{D}_V is a self-adjoint operator with essential spectrum supported on $(-\infty, -1] \cup [1, \infty)$. Depending on V(r), the spectrum may also contain discrete eigenvalues in (-1, 1). Generally, in computational chemistry, positive eigenvalues correspond to bound states of a relativistic quantum electron in the external field V, and negative eigenvalues correspond to bound states of a positron [107].

7.3.3. Computing Eigenvalues while Avoiding Spectral Pollution. Assuming that f in (7.4) is not orthogonal to any of the eigenfunctions, it follows from (7.4) and (7.5) that the positions of the peaks of the function

$$\nu_f^{\epsilon}(x) := \epsilon \cdot \operatorname{Im} (\langle \mathcal{R}_{\mathcal{D}_V}(x + i\epsilon) f, f \rangle)$$

correspond to the eigenvalues. To test this, we consider the case of $\kappa = -1$ and the Coulomb-type potentials $V(r) = \gamma/r$ for $-\sqrt{3}/2 < \gamma < 0$. For these potentials, the eigenvalues are known analytically as [107, Chap. 7]

$$E_j(\mathcal{D}_V) = \left(1 + \gamma^2 (j + \sqrt{1 - \gamma^2})^{-2}\right)^{-1/2}, \quad j \ge 0.$$

Note that the eigenvalues accumulate at 1. This makes computing $E_j(\mathcal{D}_V)$ difficult when j is large, even in the absence of spectral pollution.

Figure 7.5 (left) shows ν_f^{ϵ} with $\epsilon = 10^{-10}$, $f(r) = (\sqrt{2}re^{-r}, \sqrt{2}re^{-r})$, and $\gamma = -0.8$. One can robustly compute ν_f^{ϵ} for a fixed $\epsilon > 0$ using the techniques in subsection 6.1 and adaptively selecting the discretization size. For $\epsilon = 10^{-10}$, we can accurately compute $E_1(\mathcal{D}_V), \ldots, E_{1000}(\mathcal{D}_V)$ by the location of the local maxima of ν_f^{ϵ} . Moreover, the sizes of the peaks correspond to $\|\mathcal{P}_{E_j}f\|^2$. Figure 7.5 (left) shows that $\|\mathcal{P}_{E_j}f\|^2$ decreases at an algebraic rate as $j \to \infty$. If one is not satisfied with the accuracy of the computed eigenvalues, then one can decrease ϵ at the expense of an increased computational cost. In Figure 7.5 (right), we show the absolute error in the computed eigenvalues $E_j(\mathcal{D}_V)$ for j=0,5,10,100,500, and 1000 as $\epsilon \downarrow 0$. We find that our algorithm can resolve hundreds of eigenvalues, even when highly clustered, to an accuracy of essentially machine precision.

8. Conclusions and Additional Potential Applications. In this paper, we have developed a general framework for evaluating smoothed approximations to the spectral measures of self-adjoint operators. We have highlighted the theoretical and practical aspects of the algorithm in the contexts of differential, integral, and lattice operators. The resolvent-based framework robustly captures discrete and continuous spectral properties of the operator, rather than any underlying discretizations, yielding a flexible and efficient method for a variety of spectral problems.

A general computational framework for computing the spectral measure μ_f opens the door to a new set of algorithms for computing with operators and studying their spectral properties. As spectral characterizations of continuous and discrete models attract renewed interest in the context of data-centered applications, our algorithms may be useful in understanding the behavior of large real-world networks and new random graph models. The development of rational kernels and corresponding local evaluation schemes may also be useful for local explorations of the spectral density of operators of large finite dimension, such as in DOS calculations in physics [70] or real-world networks [29].

Our framework can be used to compute the vector-valued functional calculus via

$$F(\mathcal{L})f \approx \frac{-1}{2\pi i} \int_{-\infty}^{\infty} F(y) \sum_{j=1}^{m} \left[\alpha_j \mathcal{R}_{\mathcal{L}}(y - \epsilon a_j) f - \beta_j \mathcal{R}_{\mathcal{L}}(y - \epsilon b_j) f \right] dy,$$

which is useful in the solution of time-evolution problems. For example, taking $F(y) = \exp(-ity)$ gives an approximation of the solution to the linear Schrödinger equation with initial state f at time t. The vector-valued functional calculus may also be used to solve more complicated evolution systems, such as nonautonomous Cauchy problems and nonlinear problems, through splitting methods [72, 74]. Therefore, our approach may aid the development of discretization-oblivious exponential integrators for PDEs or sampling from stochastic processes with self-adjoint generators [58, Chap. 17].

Appendix A. Convergence Rates and Error Bounds. In this appendix, we prove the pointwise and L^p convergence bounds of $K_{\epsilon} * \mu_f$ to ρ_f as $\epsilon \downarrow 0$.

A.1. Pointwise Error Bounds. The pointwise convergence shows that samples of $K_{\epsilon} * \mu_f$ are meaningful because they converge to ρ_f , at a rate determined by the local regularity of ρ_f and the order of the kernel. Recall that in Theorem 5.2, K is an mth-order kernel, the measure μ_f is absolutely continuous on $I = (x_0 - \eta, x_0 + \eta)$ for $\eta > 0$ and a fixed $x_0 \in \mathbb{R}$, and that $\rho_f \in \mathcal{C}^{n,\alpha}(I)$ with $\alpha \in [0,1)$.

Proof of Theorem 5.2. First, we decompose ρ_f into two nonnegative parts $\rho_f = \rho_1 + \rho_2$, where ρ_1 is compactly supported on I and ρ_2 vanishes on $(x_0 - \eta/2, x_0 + \eta/2)$. Using the convolution representation for $K_{\epsilon} * \mu_f$, we have

$$(\mathrm{A.1}) \ |\rho_f(x_0) - [K_\epsilon * \mu_f](x_0)| \leq \left| \int_{\mathbb{R}} K_\epsilon(y) \left(\rho_1(x_0 - y) - \rho_1(x_0) \right) dy \right| + \left| \left[K_\epsilon * \mu_f^{(\mathrm{r})} \right] (x_0) \right|.$$

Here, the measure $d\mu_f^{(r)}(y) = d\mu_f(y) - \rho_1(y)dy$ is nonnegative and supported in the complement of $(x_0 - \eta/2, x_0 + \eta/2)$. Since μ_f is a probability measure, we have that $\int_{\mathbb{R}} d\mu_f^{(r)}(y) \leq 1$, and the second term on the right-hand side of (A.1) is bounded by

$$(A.2) \quad \left| \left[K_{\epsilon} * \mu_f^{(r)} \right] (x_0) \right| = \left| \int_{\mathbb{R}} K_{\epsilon}(x_0 - y) d\mu_f^{(r)}(y) \right| \le \sup_{|y| \ge \eta/2} |K_{\epsilon}(y)| \le \frac{C_K \epsilon^m}{(\epsilon + \frac{\eta}{2})^{m+1}},$$

where the constant C_K is given in Definition 5.1.

To bound the first term in (A.1), we expand $\rho_1(x_0 - y)$ using Taylor's theorem:

(A.3)
$$\rho_1(x_0 - y) = \sum_{j=0}^{k-1} \frac{(-1)^j \rho_1^{(j)}(x_0)}{j!} y^j + (-1)^k \frac{\rho_1^{(k)}(\xi_y)}{k!} y^k, \qquad k = \min(n, m),$$

where $|\xi_y - x_0| \le |y|$. We consider two cases separately.

Case (i): $n + \alpha < m$. In this case k = n and we can select ρ_1 so that

$$\frac{1}{n!} \left| \rho_1^{(n)} \right|_{\mathcal{C}^{0,\alpha}(I)} \le C(n,\alpha) \|\rho_f\|_{\mathcal{C}^{n,\alpha}(I)} \left(1 + \eta^{-n-\alpha} \right)$$

for some universal constant $C(n, \alpha)$ that depends only on n and α . Existence of such a decomposition follows from standard arguments with cutoff functions. Plugging (A.3) into (A.1) and applying the vanishing moment condition (Definition 5.1 (ii)), we obtain

(A.4)
$$\int_{\mathbb{R}} K_{\epsilon}(y) \left(\rho_1(x_0 - y) - \rho_1(x_0) \right) dy = (-1)^n \int_{\mathbb{R}} K_{\epsilon}(y) \frac{\rho_1^{(n)}(\xi_y)}{n!} y^n dy.$$

Since n < m, we can use the vanishing moment condition again to obtain

(A.5)
$$\int_{\mathbb{R}} K_{\epsilon}(y) \frac{\rho_1^{(n)}(\xi_y)}{n!} y^n \, dy = \int_{\mathbb{R}} K_{\epsilon}(y) \frac{\rho_1^{(n)}(\xi_y) - \rho_1^{(n)}(x_0)}{n!} y^n \, dy.$$

Since $\rho_1^{(n)} \in \mathcal{C}^{0,\alpha}(I)$ and $|\xi_y - x_0| \le |y|$, we have $|\rho_1^{(n)}(\xi_y) - \rho_1^{(n)}(x_0)| \le |\rho_1^{(n)}|_{\mathcal{C}^{0,\alpha}(I)}|y|^{\alpha}$. Applying this bound to the integrand in (A.5) and changing variables $y \to \epsilon y$,

(A.6)
$$\left| \int_{\mathbb{R}} K_{\epsilon}(y) \frac{\rho_{1}^{(n)}(\xi_{y}) - \rho_{1}^{(n)}(x_{0})}{n!} y^{n} dy \right| \leq \frac{\epsilon^{n+\alpha}}{n!} \left| \rho_{1}^{(n)} \right|_{\mathcal{C}^{0,\alpha}(I)} \int_{\mathbb{R}} |K(y)| |y|^{n+\alpha} dy.$$

Recalling our selection of ρ_1 and combining (A.6) with (A.2) proves Case (i).

Case (ii): $n + \alpha \ge m$. In this case k = m and we can select ρ_1 such that

$$2e \left\| \rho_1^{(m)} \right\|_{\infty} \le C(m) \|\rho_f\|_{\mathcal{C}^m(I)} \left(1 + \eta^{-m} \right)$$

for some universal constant C(m) that only depends on m. Again, existence of such a decomposition follows from standard arguments with cutoff functions. Since ρ_1 has compact support in I, we have that $\rho_1(x_0 - y) = 0$ if $|y| \ge \eta$. We split the range of integration in (A.4), substitute the Taylor expansion in (A.3), and change variables $y \to \epsilon y$ to obtain

(A.7)
$$\left| \int_{\mathbb{R}} K_{\epsilon}(y) \left(\rho_{1}(x_{0} - y) - \rho_{1}(x_{0}) \right) dy \right| \leq \left| \rho_{1}(x_{0}) \right| \left| \int_{|y| \geq \eta/\epsilon} K(y) dy \right|$$

$$+ \sum_{j=1}^{m-1} \frac{\epsilon^{j}}{j!} \left| \rho_{1}^{(j)}(x_{0}) \right| \left| \int_{|y| < \eta/\epsilon} K(y) y^{j} dy \right| + \frac{\epsilon^{m}}{m!} \left\| \rho_{1}^{(m)} \right\|_{\infty} \int_{|y| < \eta/\epsilon} |K(y)| |y|^{m} dy.$$

By the vanishing moment condition (see Definition 5.1 (ii)), we have that

(A.8)
$$\left| \int_{|y| < \eta/\epsilon} K(y) y^j \, dy \right| = \left| \int_{|y| \ge \eta/\epsilon} K(y) y^j \, dy \right|, \qquad 1 \le j \le m - 1.$$

Definition 5.1 (iii) implies that $|K(x)||x|^{m+1} \leq |K(x)|(1+|x|)^{m+1} \leq C_K$. Substituting (A.8) into (A.7) with the bound for |K(x)| and integrating yields an upper bound for the right-hand side of (A.7):

(A.9)
$$\sum_{j=0}^{m-1} \frac{\epsilon^{j}}{j!} \left| \rho_{1}^{(j)}(x_{0}) \right| \frac{2C_{K}}{m-j} \left(\frac{\epsilon}{\eta} \right)^{m-j} + \frac{\epsilon^{m}}{m!} \left\| \rho_{1}^{(m)} \right\|_{\infty} \int_{|y| < \eta/\epsilon} |K(y)| |y|^{m} dy.$$

Since we can write $\rho_1^{(j)}(x_0)$ as an iterated integral of $\rho_1^{(m)}$, we find that

$$\rho_1^{(j)}(x_0) = \int_{x_0 - \eta}^{x_0} \int_{x_0 - \eta}^{t_1} \cdots \int_{x_0 - \eta}^{t_{m-j-1}} \rho_1^{(m)}(t_{m-j}) dt_{m-j} \cdots dt_1, \qquad 0 \le j \le m - 1,$$

and so it follows that $|\rho_1^{(j)}(x_0)| \leq \eta^{m-j} ||\rho_1^{(m)}||_{\infty}$. Thus, we have

(A.10)
$$\sum_{j=0}^{m-1} \frac{\epsilon^{j}}{j!} \left| \rho_{1}^{(j)}(x_{0}) \right| \frac{2C_{K}}{m-j} \left(\frac{\epsilon}{\eta} \right)^{m-j} \leq 2eC_{K} \|\rho_{1}^{(m)}\|_{\infty} \epsilon^{m}.$$

Recalling our selection of ρ_1 , Case (ii) follows from (A.2), (A.9), and (A.10).

A.2. L^p Error Bounds. In subsection 5.2 we motivated error bounds for $\|\rho_f - K_\epsilon * \mu_f\|_{L^1}$ to ensure that the calculation of ionization probabilities is meaningful. In this subsection, we prove the L^p error bounds stated in Theorem 5.3. It is often easier to prove these kinds of results in Fourier space, so we begin by understanding the regularity properties of \widehat{K} for an mth-order kernel (see Definition 5.1), where

(A.11)
$$\widehat{K}(\omega) := \int_{\mathbb{R}} K(x)e^{-2\pi ix\omega} dx, \qquad \omega \in \mathbb{R}$$

LEMMA A.1 (regularity of Fourier transform). Let K be an mth-order kernel (see Definition 5.1). For any $\alpha \in (0,1)$, we have that $\widehat{K} \in \mathcal{C}^{m-1,\alpha}(\mathbb{R})$ and

(A.12)
$$|\widehat{K}(\omega) - 1| \le \frac{|\widehat{K}^{(m-1)}|_{\mathcal{C}^{0,\alpha}}}{(m-1)!} |\omega|^{m-1+\alpha}.$$

Proof. Using (5.1) we can differentiate through the integral sign in (A.11) to conclude that \hat{K} is (m-1)-times continuously differentiable. Moreover, (5.1) implies that $\hat{K}^{(m-1)} \in \mathcal{W}^{s,2}(\mathbb{R})$ for any s < 3/2 (see [75] for the definition of fractional Sobolev spaces). Therefore, $\hat{K} \in \mathcal{C}^{m-1,\alpha}(\mathbb{R})$ for any $\alpha \in (0,1)$ [75, Thm. 3.26].

For (A.12), note that the normalization condition (Definition 5.1 (i)) implies that $\widehat{K}(0) = 1$, while the vanishing moment criterion (Definition 5.1 (ii)) implies that $(\widehat{K})^{(j)}(0) = (-2\pi i)^j \int_{\mathbb{R}} K(x) x^j dx = 0$ for $1 \leq j \leq m-1$. The bound (A.12) then follows by using the (m-1)th-order Taylor expansion for \widehat{K} at the origin and applying the Hölder condition to the remainder.

We can now use this to bound the L^p error of a smoothed approximation $K_{\epsilon} * g$ when $g \in \mathcal{W}^{m,p}(\mathbb{R})$ and has compact support.

LEMMA A.2. Let K be an mth-order kernel and let g be any function such that $g \in W^{m,p}(\mathbb{R})$ for $1 \leq p < \infty$ and $\operatorname{supp}(g) \subset I = (a - \eta, b + \eta)$ for some $\eta > 0$. Then, for any $\epsilon > 0$, we have that 1^{14}

(A.13)
$$||[K_{\epsilon} * g] - g||_{L^{p}(I)} \le \frac{2\epsilon^{m} C_{K}}{m!} ||g^{(m)}||_{L^{p}(\mathbb{R})} \log(1 + (b - a + 2\eta)/\epsilon).$$

 $^{^{14}}$ The $\log(1/\epsilon)$ factor is avoided if extra decay—beyond Definition 5.1 (iii)—is assumed on K.

Proof. Since $K \in L^1(\mathbb{R})$, we can define the function

(A.14)
$$\phi_1(x) = \int_{-\infty}^x K(y)dy - H(x) \int_{\mathbb{R}} K(y)dy = \begin{cases} \int_{-\infty}^x K(y)dy, & x < 0, \\ -\int_x^\infty K(y)dy, & x > 0, \end{cases}$$

where H(x) denotes the Heaviside step function. Using (5.1) and integrating directly, we see that $\phi_1 \in L^2(\mathbb{R})$. Furthermore, since $\int_{\mathbb{R}} K(y)dy = 1$, we can differentiate ϕ_1 in the sense of tempered distributions to obtain $\phi'_1 = K - \delta_0$. Taking Fourier transforms, we see that

$$(2\pi i\omega)\widehat{\phi}_1(\omega) = \widehat{K}(\omega) - 1.$$

However, $\widehat{\phi}_1, \widehat{K} \in L^2(\mathbb{R})$, and hence we must have $\widehat{\phi}_1(\omega) = (\widehat{K}(\omega) - 1)(2\pi i\omega)^{-1}$ almost everywhere, and in particular that $(\widehat{K}(\omega) - 1)(2\pi i\omega)^{-1} \in L^2(\mathbb{R})$.

If m > 1, then by (5.1) and the case definition of ϕ_1 in (A.14), we have $\phi_1 \in L^1(\mathbb{R})$, and hence $\widehat{\phi}_1$ can be identified with a continuous function. Furthermore, (A.12) implies that $\widehat{\phi}_1(0) = \int_{\mathbb{R}} \phi_1(y) dy = 0$, and hence we can define

$$\phi_2(x) = \int_{-\infty}^x \phi_1(y) dy - H(x) \int_{\mathbb{R}} \phi_1(y) dy = \begin{cases} \int_{-\infty}^x \phi_1(y) dy, & x < 0, \\ -\int_x^\infty \phi_1(y) dy, & x > 0. \end{cases}$$

Again by using (5.1) and integrating directly, we see that $\phi_2 \in L^2(\mathbb{R})$. We can take distributional derivatives and Fourier transforms as before to deduce that $\hat{\phi}_2(\omega) = (\hat{K}(\omega) - 1)(2\pi i\omega)^{-2}$ almost everywhere. We continue this argument inductively, using Lemma A.1, and for $j = 2, \ldots, m$ we define $\phi_j(x) = \int_{-\infty}^x \phi_{j-1}(y) dy$. The argument shows that $\hat{\phi}_j(\omega) = (\hat{K}(\omega) - 1)(2\pi i\omega)^{-j}$. Using (5.1) and integrating, we have

(A.15)
$$|\phi_j(x)| \le C_K(m-j)!/(m!(1+|x|)^{m-j+1}), \qquad 1 \le j \le m.$$

Let $g_n \in C_c^{\infty}(\mathbb{R})$ for $n \geq 1$ be a sequence of functions with $\operatorname{supp}(g_n) \subseteq (a - \eta - n^{-1}, b + \eta + n^{-1})$ such that $\|g - g_n\|_{\mathcal{W}^{m,p}(\mathbb{R})} \to 0$ as $n \to \infty$. Let $\phi_{m,\epsilon} = \epsilon^{-1}\phi_m(x\epsilon^{-1})$, so that

$$\widehat{\phi}_{m,\epsilon}(\omega) = \frac{\widehat{K}_{\epsilon}(\omega) - 1}{(2\pi i \epsilon \omega)^m}.$$

It follows, by the convolution theorem and Carleson's theorem, that for a.e. $x \in \mathbb{R}$ (A.16)

$$[K_{\epsilon} * g_n](x) - g_n(x) = \int_{\mathbb{R}} \frac{\widehat{K}_{\epsilon}(\omega) - 1}{(2\pi i \omega)^m} (2\pi i \omega)^m \widehat{g}_n(\omega) e^{2\pi i \omega x} d\omega = \epsilon^m [\phi_{m,\epsilon} * g_n^{(m)}](x).$$

Letting $L_n = ((b-a) + 2(\eta + n^{-1}))$, we have $[\phi_{m,\epsilon} * g_n^{(m)}](x) = [\chi_{[-L_n,L_n]}\phi_{m,\epsilon} * g_n^{(m)}](x)$ for $x \in I$, where χ_U denotes the indicator function of a set U. Moreover, $\chi_{[-L_n,L_n]}\phi_{m,\epsilon} \in L^1(\mathbb{R})$ by Hölder's inequality. Taking the L^p norm on both sides of (A.16) and applying Young's convolution inequality yields

(A.17)
$$||[K_{\epsilon} * g_n] - g_n||_{L^p(I)} \le \epsilon^m ||g_n^{(m)}||_{L^p(\mathbb{R})} ||\phi_{m,\epsilon}||_{L^1([-L_n, L_n])}.$$

By taking the limit $n \to \infty$ in (A.17), we have that

(A.18)
$$||[K_{\epsilon} * g] - g||_{L^{p}(I)} \le \epsilon^{m} ||g^{(m)}||_{L^{p}(\mathbb{R})} \int_{|y| \le (b-a)+2\eta} |\phi_{m,\epsilon}(y)| \, dy.$$

Finally, by (A.15) with j=m, we have that $|\phi_{m,1}(x)| \leq C_K (m!(1+|x|))^{-1}$. Changing variables $y \to \epsilon y$ in the last integral in (A.18), applying the bound for $\phi_{m,1}$, and integrating yields the upper bound in (A.13).

We are now ready to prove the L^p error bounds when $1 \le p < \infty$.

Proof of Theorem 5.3. Let $I' = (a - \eta/2, b + \eta/2)$. Since $\rho_f|_I \in \mathcal{W}^{m,p}(I)$, we can decompose $\rho_f = \rho_1 + \rho_2$ such that ρ_1 is nonnegative, supported in I with $2\|\rho_1^{(m)}\|_{L^p(\mathbb{R})}/m! \le C(m)\|\rho_f\|_{\mathcal{W}^{m,p}(I)}(1+\eta^{-m})$ for some constant C(m) (that depends only on m), and ρ_2 is nonnegative with support contained in $\mathbb{R} \setminus I'$. Therefore, $\rho_f = \rho_1$ on (a,b) and

$$(A.19) \|\rho_f - K_{\epsilon} * \mu_f\|_{L^p((a,b))} \le \|\rho_1 - K_{\epsilon} * \rho_1\|_{L^p((a,b))} + \|K_{\epsilon} * \rho_1 - K_{\epsilon} * \mu_f\|_{L^p((a,b))}.$$

The first term is bounded via Lemma A.2. To bound the second term, we note that the measure $\mu_f^{(r)} = \mu_f - \rho_1$ is nonnegative, supported in $\mathbb{R} \setminus I'$, and has $\int_{\mathbb{R}} d\mu_f^{(r)}(y) \leq 1$. Applying property (iii) in Definition 5.1, we see that

$$||K_{\epsilon} * \rho_{1} - K_{\epsilon} * \mu_{f}||_{L^{p}((a,b))}^{p} \leq \int_{a}^{b} \left(\epsilon^{-1} \int_{\mathbb{R}\backslash I'} |K((x-y)/\epsilon)| d\mu^{(r)}(y) \right)^{p} dx$$
$$\leq C_{K}^{p}(b-a)(\epsilon + \eta/2)^{-(m+1)p} \epsilon^{mp}.$$

Combining the bounds for the terms in (A.19) concludes the proof.

Acknowledgments. The authors are grateful to St. John's College, Cambridge, for funding the first author to visit Cornell University, during which this collaboration started. They thank Anthony Austin and Mikael Slevinsky for carefully reading a draft of this manuscript, and the referees, whose careful comments helped improve it.

REFERENCES

- A. AGAZZI, J.-P. ECKMANN, AND G. M. GRAF, The colored Hofstadter butterfly for the honeycomb lattice, J. Stat. Phys., 156 (2014), pp. 417–426. (Cited on p. 511)
- [2] W. O. Amrein and V. Georgescu, Characterization of Bound States and Scattering States in Quantum Mechanics, tech. report, University of Geneva, 1973. (Cited on p. 492)
- [3] A. AVILA AND S. JITOMIRSKAYA, The ten martini problem, Ann. of Math. (2), 170 (2009), pp. 303-342. (Cited on p. 496)
- [4] Z. Bai and J. W. Silverstein, Spectral Analysis of Large Dimensional Random Matrices, Springer Ser. Statist. 20, Springer, 2010. (Cited on p. 493)
- [5] N. BEER AND D. G. PETTIFOR, The recursion method and the estimation of local densities of states, in The Electronic Structure of Complex Systems, Springer, 1984, pp. 769–777. (Cited on pp. 490, 493)
- [6] P. BILLINGSLEY, Convergence of Probability Measures, 2nd ed., John Wiley & Sons, 1999. (Cited on p. 492)
- [7] D. BILMAN AND T. TROGDON, Numerical inverse scattering for the Toda lattice, Comm. Math. Phys., 352 (2017), pp. 805–879. (Cited on p. 494)
- [8] A. BÖTTCHER AND B. SILBERMANN, Introduction to Large Truncated Toeplitz Matrices, Springer-Verlag, New York, 1999. (Cited on p. 492)
- [9] J. P. BOYD, Chebyshev and Fourier Spectral Methods, Courier Corporation, 2001. (Cited on pp. 490, 509)
- [10] R. CARMONA AND J. LACROIX, Spectral Theory of Random Schrödinger Operators, Prob. Appl., Birkhäuser Boston, 1990. (Cited on p. 493)
- [11] A. H. CASTRO NETO, F. GUINEA, N. M. R. PERES, K. S. NOVOSELOV, AND A. K. GEIM, The electronic properties of graphene, Rev. Modern Phys., 81 (2009), pp. 109–162. (Cited on p. 511)
- [12] K. Chang, A physics magic trick: Take 2 sheets of carbon and twist, The New York Times, 2019, https://www.nytimes.com/2019/10/30/science/graphene-physics-superconductor. html. (Cited on p. 511)

- [13] F. CHATELIN, Spectral Approximation of Linear Operators, Academic Press, 1983. (Cited on p. 490)
- [14] T. S. CHIHARA, An Introduction to Orthogonal Polynomials, Gordon and Breach, New York, London, Paris, 1978. (Cited on p. 494)
- [15] E. A. CODDINGTON AND N. LEVINSON, Theory of Ordinary Differential Equations, Krieger, Malabar, FL, 1984. (Cited on p. 494)
- [16] M. J. COLBROOK, Computing spectral measures and spectral types, Comm. Math. Phys., 384 (2021), pp. 433-501. (Cited on pp. 490, 496, 508, 510)
- [17] M. J. COLBROOK, The Foundations of Infinite-Dimensional Spectral Computations, Ph.D. thesis, University of Cambridge, 2020. (Cited on p. 496)
- [18] M. J. COLBROOK AND A. C. HANSEN, The Foundations of Spectral Computations via the Solvability Complexity Index Hierarchy: Part I, preprint, https://arxiv.org/abs/1908. 09592, 2019. (Cited on p. 496)
- [19] M. J. COLBROOK AND A. C. HANSEN, On the infinite-dimensional QR algorithm, Numer. Math., 143 (2019), pp. 17–83. (Cited on p. 496)
- [20] M. J. COLBROOK, A. HORNING, AND A. TOWNSEND, SpecSolve, GitHub, https://github.com/ SpecSolve, 2020. (Cited on p. 491)
- [21] M. J. COLBROOK, B. ROMAN, AND A. C. HANSEN, How to compute spectra with error control, Phys. Rev. Lett., 122 (2019), art. 250201, https://doi.org/10.1103/PhysRevLett.122. 250201. (Cited on pp. 513, 514)
- [22] H. CRAMÉR, On some classes of nonstationary stochastic processes, in Proceedings of the Fourth Berkeley Symposium on Mathematical Statistics and Probability, Vol. 2, University of Los Angeles Press, Berkeley, Los Angeles, 1961, pp. 57–78. (Cited on p. 493)
- [23] D. Damanik, Singular continuous spectrum for a class of substitution Hamiltonians, Lett. Math. Phys., 46 (1998), pp. 303–311. (Cited on p. 496)
- [24] D. DAMANIK, M. EMBREE, AND A. GORODETSKI, Spectral properties of Schrödinger operators arising in the study of quasicrystals, in Mathematics of Aperiodic Order, Springer, 2015, pp. 307–370. (Cited on p. 496)
- [25] D. DAMANIK AND B. SIMON, Jost functions and Jost solutions for Jacobi matrices, I. A necessary and sufficient condition for Szegő asymptotics, Invent. Math., 165 (2006), pp. 1– 50. (Cited on p. 490)
- [26] P. Deift, Orthogonal Polynomials and Random Matrices: A Riemann-Hilbert Approach, Courant Lecture Notes 3, AMS, Providence, RI, 1999. (Cited on p. 494)
- [27] F. Dell'Oro and V. Pata, Second order linear evolution equations with general dissipation, Appl. Math. Opt., 2019, https://doi.org/10.1007/s00245-019-09613-x. (Cited on p. 493)
- [28] J. DOMBROWSKI AND P. NEVAI, Orthogonal polynomials, measures and recurrence relations, SIAM J. Math. Anal., 17 (1986), pp. 752–759, https://doi.org/10.1137/0517054. (Cited on pp. 490, 494)
- [29] K. Dong, A. R. Benson, and D. Bindel, Network density of states, in Proceedings of the 25th ACM SIGKDD International Conference on Knowledge Discovery & Data Mining, 2019, pp. 1152–1161. (Cited on p. 516)
- [30] G. W. F. DRAKE AND S. P. GOLDMAN, Application of discrete-basis-set methods to the Dirac equation, Phys. Rev. A, 23 (1981), art. 2093. (Cited on p. 514)
- [31] N. Dunford and J. T. Schwartz, Linear Operators: Part II: Spectral Theory: Self Adjoint Operators in Hilbert Space, Interscience, 1963. (Cited on p. 492)
- [32] K. G. DYALL AND K. FÆGRI, JR., Kinetic balance and variational bounds failure in the solution of the Dirac equation in a finite Gaussian basis set, Chem. Phys. Lett., 174 (1990), pp. 25–32. (Cited on p. 514)
- [33] V. D. EFROS, W. LEIDEMANN, AND G. ORLANDINI, Response functions from integral transforms with a Lorentz kernel, Phys. Lett. B, 338 (1994), pp. 130–133. (Cited on pp. 490, 492)
- [34] V. D. EFROS, W. LEIDEMANN, G. ORLANDINI, AND N. BARNEA, The Lorentz integral transform (LIT) method and its applications to perturbation-induced reactions, J. Phys. G, 34 (2007), art. R459. (Cited on pp. 490, 493)
- [35] V. D. EFROS, W. LEIDEMANN, AND V. Y. SHALAMOVA, On calculating response functions via their Lorentz integral transforms, Few-Body Syst., 60 (2019), art. 35. (Cited on p. 490)
- [36] V. Enss, Asymptotic completeness for quantum mechanical potential scattering, Comm. Math. Phys., 61 (1978), pp. 285–291. (Cited on p. 492)
- [37] L. C. EVANS, Partial Differential Equations, 2nd ed., Grad. Stud. Math. 19, AMS, 2010. (Cited on pp. 497, 498, 506)
- [38] K. O. FRIEDRICHS, On the perturbation of continuous spectra, Commun. Pure Appl. Math., 1 (1948), pp. 361–406. (Cited on p. 492)

- [39] C. FULTON, D. PEARSON, AND S. PRUESS, Computing the spectral function for singular Sturm– Liouville problems, J. Comput. Appl. Math., 176 (2005), pp. 131–162. (Cited on p. 494)
- [40] C. FULTON, D. PEARSON, AND S. PRUESS, New characterizations of spectral density functions for singular Sturm-Liouville problems, J. Comput. Appl. Math., 212 (2008), pp. 194–213. (Cited on p. 494)
- [41] C. FULTON AND S. PRUESS, The computation of spectral density functions for singular Sturm– Liouville problems involving simple continuous spectra, ACM Trans. Math. Soft., 24 (1998), pp. 107–129. (Cited on p. 494)
- [42] C. FULTON, S. PRUESS, AND W. SHOAFF, Parallel computation of Sturm-Liouville spectral density functions, Parallel Algorithms Appl., 4 (1994), pp. 41–51. (Cited on p. 494)
- [43] F. GAMBOA, J. NAGEL, AND A. ROUAULT, Sum rules via large deviations, J. Funct. Anal., 270 (2016), pp. 509–559. (Cited on p. 494)
- [44] V. GIRARDIN AND R. SENOUSSI, Semigroup stationary processes and spectral representation, Bernoulli, 9 (2003), pp. 857–876. (Cited on pp. 490, 493)
- [45] I. M. GLAZMAN, Direct Methods of Qualitative Spectral Analysis of Singular Differential Operators, Israel Program for Scientific Translations, 1965. (Cited on p. 492)
- [46] A. Y. GORDON, S. JITOMIRSKAYA, Y. LAST, AND B. SIMON, Duality and singular continuous spectrum in the almost Mathieu equation, Acta Math., 178 (1997), pp. 169–183. (Cited on p. 496)
- [47] K. Gustafson, Operator spectral states, Comput. Math. Appl., 34 (1997), pp. 467–508. (Cited on p. 490)
- [48] B. C. Hall, Quantum Theory for Mathematicians, Grad. Texts in Math. 267, Springer, 2013. (Cited on p. 492)
- [49] M. HAMZAVI, K.-E. THYLWE, AND A. RAJABI, Approximate bound states solution of the Hellmann potential, Commun. Theoret. Phys., 60 (2013), pp. 1–8. (Cited on p. 506)
- [50] R. HAYDOCK, V. HEINE, AND M. J. KELLY, Electronic structure based on the local atomic environment for tight-binding bands, J. Phys. C Solid State Phys., 5 (1972), pp. 2845– 2858. (Cited on pp. 490, 493)
- [51] H. HELLMANN, A new approximation method in the problem of many electrons, J. Chem. Phys., 3 (1935), p. 61. (Cited on p. 506)
- [52] M. HOCHBRUCK AND A. OSTERMANN, Exponential integrators, Acta Numer., 19 (2010), pp. 209–286. (Cited on p. 490)
- [53] K. HOFFMAN, Banach Spaces of Analytic Functions, Prentice-Hall, 1962. (Cited on p. 497)
- [54] D. R. HOFSTADTER, Energy levels and wave functions of Bloch electrons in rational and irrational magnetic fields, Phys. Rev. B, 14 (1976), pp. 2239–2249. (Cited on p. 513)
- [55] A. HORNING AND A. TOWNSEND, FEAST for differential eigenvalue problems, SIAM J. Numer. Anal., 58 (2020), pp. 1239–1262, https://doi.org/10.1137/19M1238708. (Cited on p. 490)
- [56] D. Hundertmark, M. Meyries, L. Machinek, and R. Schnaubelt, Operator semigroups and dispersive equations, in 16th Internet Seminar on Evolution Equations, 2013, pp. 1– 8, https://www.math.kit.edu/iana3/~schnaubelt/media/isem16-skript.pdf. (Cited on p. 493)
- [57] S. Joe, Discrete collocation methods for second kind Fredholm integral equations, SIAM J. Numer. Anal., 22 (1985), pp. 1167–1177, https://doi.org/10.1137/0722070. (Cited on p. 496)
- [58] O. Kallenberg, Foundations of Modern Probability, Springer Science & Business Media, 2006. (Cited on p. 516)
- [59] G. KALLIANPUR AND V. MANDREKAR, Spectral theory of stationary H-valued processes, J. Multivar. Anal., 1 (1971), pp. 1–16. (Cited on pp. 490, 493)
- [60] T. Kato, Perturbation Theory for Linear Operators, 2nd ed., Grundlehren Math. Wiss. 132, Springer Science & Business Media, 1976. (Cited on pp. 490, 492, 493, 496)
- [61] A. Kiejna and K. F. Wojciechowski, Metal Surface Electron Physics, Elsevier, 1996. (Cited on p. 492)
- [62] R. KILLIP AND B. SIMON, Sum rules for Jacobi matrices and their applications to spectral theory, Ann. of Math. (2), 158 (2003), pp. 253-321. (Cited on pp. 490, 494)
- [63] W. KOPPELMAN, On the spectral theory of singular integral operators, Trans. Amer. Math. Soc., 97 (1960), pp. 35–63. (Cited on p. 492)
- [64] W. KUTZELNIGG, Basis set expansion of the Dirac operator without variational collapse, Internat. J. Quant. Chem., 25 (1984), pp. 107–129. (Cited on p. 514)
- [65] W. KUTZELNIGG, Relativistic one-electron Hamiltonians for electrons only and the variational treatment of the Dirac equation, Chem. Phys., 225 (1997), pp. 203–222. (Cited on p. 514)
- [66] P. W. LANGHOFF, Stieltjes-Tchebycheff moment-theory approach to photoeffect studies in Hilbert space, in Theory and Applications of Moment Methods in Many-Fermion Systems, Springer, 1980, pp. 191–212. (Cited on p. 493)

- [67] B. M. LEVITAN AND I. S. SARGSIAN, Introduction to Spectral Theory: Selfadjoint Ordinary Differential Operators, Transl. Math. Monogr. 39, AMS, 1975. (Cited on p. 492)
- [68] M. LEWIN AND E. SÉRÉ, Spectral pollution and how to avoid it (with applications to Dirac and periodic Schrödinger operators), Proc. Lond. Math. Soc. (3), 100 (2010), pp. 864–900, https://doi.org/10.1112/plms/pdp046. (Cited on p. 514)
- [69] J. LIESEN AND Z. STRAKOS, Krylov Subspace Methods: Principles and Analysis, Oxford University Press, Oxford, 2013. (Cited on p. 494)
- [70] L. LIN, Y. SAAD, AND C. YANG, Approximating spectral densities of large matrices, SIAM Rev., 58 (2016), pp. 34–65, https://doi.org/10.1137/130934283. (Cited on pp. 490, 492, 493, 501, 516)
- [71] X. Lu, P. Stepanov, W. Yang et al., Superconductors, orbital magnets and correlated states in magic-angle bilayer graphene, Nature, 574 (2019), pp. 653–657. (Cited on p. 511)
- [72] C. Lubich, From Quantum to Classical Molecular Dynamics: Reduced Models and Numerical Analysis, Zurich Lectures in Advanced Mathematics, European Mathematical Society (EMS), Zürich, 2008. (Cited on pp. 490, 493, 511, 516)
- [73] V. A. MARCHENKO, Sturm-Liouville Operators and Applications, AMS, 2011. (Cited on p. 494)
- [74] R. I. MCLACHLAN AND G. R. W. QUISPEL, Splitting methods, Acta Numer., 11 (2002), pp. 341–434. (Cited on p. 516)
- [75] W. C. H. McLean, Strongly Elliptic Systems and Boundary Integral Equations, Cambridge University Press, 2000. (Cited on p. 518)
- [76] K. S. NOVOSELOV, Nobel lecture: Graphene: Materials in the flatland, Rev. Modern Phys., 83 (2011), pp. 837–849. (Cited on p. 511)
- [77] S. OLVER AND A. TOWNSEND, A fast and well-conditioned spectral method, SIAM Rev., 55 (2013), pp. 462–489, https://doi.org/10.1137/120865458. (Cited on p. 509)
- [78] E. PARZEN, On consistent estimates of the spectrum of a stationary time series, Ann. Math. Stat., 28 (1957), pp. 329–348. (Cited on p. 494)
- [79] E. PARZEN, Mathematical considerations in the estimation of spectra, Technometrics, 3 (1961), pp. 167–190. (Cited on p. 494)
- [80] E. Parzen, On estimation of a probability density function and mode, Ann. Math. Statist., 33 (1962), pp. 1065–1076. (Cited on p. 494)
- [81] A. PAZY, Semigroups of Linear Operators and Applications to Partial Differential Equations, Appl. Math. Sci. 44, Springer Science & Business Media, 2012. (Cited on p. 493)
- [82] L. A. PONOMARENKO, R. V. GORBACHEV, G. L. YU, D. C. ELIAS, R. JALIL, A. A. PATEL, A. MISHCHENKO, A. S. MAYOROV, C. R. WOODS, J. R. WALLBANK ET AL., Cloning of Dirac fermions in graphene superlattices, Nature, 497 (2013), pp. 594–597. (Cited on p. 511)
- [83] M. B. PRIESTLEY, Basic considerations in the estimation of spectra, Technometrics, 4 (1962), pp. 551–564. (Cited on p. 494)
- [84] S. PRUESS AND C. T. FULTON, Mathematical software for Sturm-Liouville problems, ACM Trans. Math. Soft., 19 (1993), pp. 360-376. (Cited on p. 494)
- [85] S. PRUESS AND C. T. FULTON, Error analysis in the approximation of Sturm-Liouville spectral density functions, J. Math. Anal. Appl., 203 (1996), pp. 518-539. (Cited on p. 494)
- [86] C. Puelz, M. Embree, and J. Fillman, Spectral approximation for quasiperiodic Jacobi operators, Integral Equations Operator Theory, 82 (2015), pp. 533–554. (Cited on p. 496)
- [87] M. REED AND B. SIMON, Methods of Modern Mathematical Physics. I, 2nd ed., Academic Press, Harcourt Brace Jovanovich, New York, 1980. (Cited on pp. 491, 492, 494, 495)
- [88] M. ROSENBLATT, Remarks on some nonparametric estimates of a density function, Ann. Math. Statist., 27 (1956), pp. 832–837. (Cited on p. 494)
- [89] M. ROSENBLATT, Stochastic Curve Estimation, NSF-CBMS Reg. Conf. Ser. Probab. Statist. 3, Institute of Mathematical Statistics, 1991. (Cited on pp. 490, 493)
- [90] D. RUELLE, A remark on bound states in potential-scattering theory, Nuovo Cimento A (10), 61 (1969), pp. 655–662. (Cited on p. 492)
- [91] V. M. Shabaev, I. I. Tupitsyn, V. A. Yerokhin, G. Plunien, and G. Soff, Dual kinetic balance approach to basis-set expansions for the Dirac equation, Phys. Rev. Lett., 93 (2004), art. 130405. (Cited on p. 514)
- [92] R. N. SILVER AND H. RÖDER, Densities of states of mega-dimensional Hamiltonian matrices, Internat. J. Modern Phys. C, 5 (1994), pp. 735–753. (Cited on p. 493)
- [93] B. W. SILVERMAN, Density Estimation for Statistics and Data Analysis, Routledge, 2018. (Cited on p. 501)
- [94] B. Simon, Schrödinger semigroups, Bull. Amer. Math. Soc., 7 (1982), pp. 447–526. (Cited on p. 493)

- [95] B. Simon, Szegő's Theorem and Its Descendants: Spectral Theory for L² Perturbations of Orthogonal Polynomials, Porter Lect. 6, Princeton University Press, 2010. (Cited on p. 494)
- [96] R. E. STANTON AND S. HAVRILIAK, Kinetic balance: A partial solution to the problem of variational safety in Dirac calculations, J. Chem. Phys., 81 (1984), pp. 1910–1918. (Cited on p. 514)
- [97] E. M. STEIN AND R. SHAKARCHI, Real Analysis: Measure Theory, Integration, and Hilbert Spaces, Princeton University Press, 2009. (Cited on p. 492)
- [98] E. M. STEIN AND R. SHAKARCHI, Functional Analysis: Introduction to Further Topics in Analysis, Princeton Lect. Anal. 4, Princeton University Press, 2011. (Cited on p. 500)
- [99] P. STOICA AND R. L. MOSES, Spectral Analysis of Signals, Pearson Prentice Hall, Upper Saddle River, NJ, 2005. (Cited on p. 493)
- [100] M. Stone and P. Goldbart, Mathematics for Physics: A Guided Tour for Graduate Students, Cambridge University Press, 2009. (Cited on p. 490)
- [101] M. H. STONE, Linear Transformations in Hilbert Space, Amer. Math. Soc. Colloq. Pub. 15, AMS, Providence, RI, 1990. (Cited on p. 495)
- [102] A. SÜTŐ, Singular continuous spectrum on a Cantor set of zero Lebesgue measure for the Fibonacci Hamiltonian, J. Statist. Phys., 56 (1989), pp. 525–531. (Cited on p. 496)
- [103] G. Szegő, Orthogonal Polynomials, AMS, New York, 1939. (Cited on p. 494)
- [104] J. D. Talman, Minimax principle for the Dirac equation, Phys. Rev. Lett., 57 (1986), pp. 1091–1094. (Cited on p. 514)
- [105] D. J. TANNOR, Introduction to Quantum Mechanics: A Time-Dependent Perspective, University Science Books, 2007. (Cited on p. 493)
- [106] G. TESCHL, Jacobi Operators and Completely Integrable Nonlinear Lattices, Math. Surv. Monogr. 72, AMS, Providence, RI, 2000. (Cited on p. 494)
- [107] B. THALLER, The Dirac Equation, Texts Monogr. Phys., Springer-Verlag, Berlin, 1992, https://doi.org/10.1007/978-3-662-02753-0. (Cited on pp. 514, 515)
- [108] E. C. TITCHMARSH, Eigenfunction Expansions Associated with Second Order Differential Equations, Part I, 2nd ed., Oxford University Press, 1962. (Cited on p. 492)
- [109] T. TOUHEI, A scattering problem by means of the spectral representation of Green's function for a layered acoustic half-space, Comput. Mech., 25 (2000), pp. 477–488. (Cited on p. 490)
- [110] A. TOWNSEND AND L. N. TREFETHEN, An extension of Chebfun to two dimensions, SIAM J. Sci. Comput., 35 (2013), pp. C495–C518, https://doi.org/10.1137/130908002. (Cited on p. 510)
- [111] L. N. TREFETHEN, Approximation Theory and Approximation Practice. Extended Edition, SIAM, Philadelphia, PA, 2019, https://doi.org/10.1137/1.9781611975949. (Cited on pp. 509, 510)
- [112] L. N. TREFETHEN AND D. BAU III, Numerical Linear Algebra, SIAM, Philadelphia, PA, 1997, https://doi.org/10.1137/1.9781611971446. (Cited on p. 512)
- [113] L. N. TREFETHEN AND J. A. C. WEIDEMAN, The exponentially convergent trapezoidal rule, SIAM Rev., 56 (2014), pp. 385–458, https://doi.org/10.1137/130932132. (Cited on p. 509)
- [114] T. TROGDON, S. OLVER, AND B. DECONINCK, Numerical inverse scattering for the Kortewegde Vries and modified Korteweg-de Vries equations, Phys. D, 241 (2012), pp. 1003–1025. (Cited on pp. 490, 494)
- [115] A. B. TSYBAKOV, Introduction to Nonparametric Estimation, Springer Science & Business Media, 2008. (Cited on pp. 494, 500, 501, 502, 507)
- [116] M. P. WAND AND M. C. JONES, Kernel Smoothing, Chapman and Hall/CRC, 1994. (Cited on pp. 494, 500)
- [117] M. WEBB AND S. OLVER, Spectra of Jacobi operators via connection coefficient matrices, Comm. Math. Phys., 382 (2021), pp. 657–707. (Cited on p. 494)
- [118] A. Weisse, G. Wellein, A. Alvermann, and H. Fehske, The kernel polynomial method, Rev. Modern Phys., 78 (2006), pp. 275–306. (Cited on p. 493)
- [119] J. WILKENING AND A. CERFON, A spectral transform method for singular Sturm-Liouville problems with applications to energy diffusion in plasma physics, SIAM J. Appl. Math., 75 (2015), pp. 350–392, https://doi.org/10.1137/130941948. (Cited on pp. 490, 494)